Aus der Klinik für **Angeborene Herzfehler Kinderkardiologie**
der Medizinischen Fakultät Charité – Universitätsmedizin Berlin

DISSERTATION

Die Anwendung der 4D-Segmentierung der Herz-CT für den prä- und postoperativen Transkatheter-Lungenklappenersatz

The application of 4D cardiac CT segmentation for pre-operative and post-operative transcatheter pulmonary valve replacement

zur Erlangung des akademischen Grades
Doctor medicinae (Dr. med.)

vorgelegt der Medizinischen Fakultät
Charité – Universitätsmedizin Berlin

von

Yimeng Hao

aus Shiyan, Hubei, Volksrepublik China

Datum der Promotion: 30.11.2023

Table of Contents

List of Figures

List of abbreviations

Two-dimension	2D
Three-dimension	3D
Four-dimension	4D
Cardiac magnetic resonance imaging	cMRI
Computed tomography angiography	CTA
Computed tomography	CT
Intra-cardiac echocardiography	ICE
Pulmonary artery	PA
Paravalvular leak	PVL
Right ventricular outflow tract	RVOT
Transcatheter pulmonary valve replacement	TPVR

Abstract (English)

Background: Transcatheter pulmonary valve replacement (TPVR) has become an alternative therapeutic option for patients with right ventricular outflow tract (RVOT) dysfunction. Cardiac CT angiography (CTA) is crucial for TPVR pre- and post-operative assessment of the landing zone from RVOT to pulmonary artery (PA). However, three-dimension (3D) CT is still inadequate to assess the full dynamic variation of landing zone and spatial relationships between structures over the cardiac cycle accurately.

Methods: The objective of this present study was to simulate the dynamic variation of the landing zone from RVOT to PA in vivo for TPVR by four-dimension (4D) CTA segmentation and evaluate the feasibility and accuracy of the 4D straightened model. The straightened model was created by adding centerline to the right heart model, then the anatomical right heart model was straightened. The 4D conventional anatomical model and straightened model were reconstructed at 10 cardiac cycle phases in 14 cardiac CTA datasets of seven sheep underwent TPVR. The cross-sectional area, circumference, and diameter deformations over the cardiac cycle were measured at five planes of the landing zone from pre- and post-operative 4D CTA. In addition, the correlation analysis between the anatomical model and straightened model was also conducted by means of Pearson correlation and Bland-Altman analysis.

Results: The clear structure of each section from RVOT to PA were observed on straightened model. Significant variations of cross-sectional area and circumference measurements showed at the RVOT plane throughout the cardiac cycle for both pre- and post-operative 4D CTA. Nevertheless, nearly no deformation of area and circumference was observed at the valvular sinuses level (Plane 3a) and the sino-tubular junction plane (Plane 4a) from pre-operative CT; the middle plane of the stent level (Plane 3b) and the top plane of the stent level (Plane 4b) from the post-operative CT. The straightened model was highly correlated with the anatomical model. The Pearson correlation coefficient between straightened model and anatomical model for cross-sectional area, circumference, minimum diameter, and maximum diameter ranged from 0.77 to 0.99 ($P < 0.0001$) and the limits of agreement from Bland-Altman analysis were within a good range, which further confirmed the great agreement between straightened model and anatomical model.

Conclusions: The 4D CT anatomical model can be used to demonstrate the deformation of RVOT to PA dynamics over the cardiac cycle. The straightened model can show the

changes in the landing area, accurately measure these data, and clearly show the structure of the various sections.

Kurzfassung (Deutsch)

Hintergrund: Der Transkatheter-Pulmonalklappenersatz (TPVR) hat sich zu einer alternativen Therapieoption für Patienten mit einer Funktionsstörung des rechtsventrikulären Ausflusstrakts (RVOT) entwickelt. Die kardiale CT-Angiographie (CTA) ist von entscheidender Bedeutung für die prä- und postoperative Beurteilung der Landezone vom RVOT zur Pulmonalarterie (PA) bei der TPVR. Die dreidimensionale (3D) CT ist jedoch noch immer unzureichend, um die vollständige dynamische Veränderung der Landezone und die räumlichen Beziehungen zwischen den Strukturen während des Herzzyklus genau zu beurteilen.

Methoden: Ziel dieser Studie war es, die dynamische Veränderung der Landezone vom RVOT zur PA in vivo für die TPVR durch vierdimensionale (4D) CTA-Segmentierung zu simulieren und die Durchführbarkeit und Genauigkeit des begradigten 4D-Modells zu bewerten. Das begradigte Modell wurde durch Hinzufügen einer Mittellinie zum Rechtsherzmodell erstellt, anschließend wurde das anatomische Rechtsherzmodell begradigt. Das konventionelle anatomische 4D-Modell und das begradigte Modell wurden in 10 Herzzyklusphasen in 14 kardialen CTA-Datensätzen von sieben Schafen rekonstruiert, die eine TPVR aufwiesen. Die Querschnittsfläche, der Umfang und die Durchmesserverformungen über den Herzzyklus wurden in fünf Ebenen der Landezone aus der prä- und postoperativen 4D-CTA gemessen. Darüber hinaus wurde die Korrelationsanalyse zwischen dem anatomischen Modell und dem begradigten Modell mittels Pearson-Korrelation und Bland-Altman-Analyse durchgeführt.

Ergebnisse: Die klare Struktur jedes Abschnitts vom RVOT bis zur PA wurde am begradigten Modell beobachtet. Sowohl bei der prä- als auch bei der postoperativen 4D-CTA zeigten sich in der RVOT-Ebene während des Herzzyklus signifikante Schwankungen der Querschnittsfläche und des Umfangs. Dennoch wurde auf der Ebene der Klappenhöhlen (Ebene 3a) und der Ebene der sino-tubulären Verbindung (Ebene 4a) im präoperativen CT nahezu keine Verformung der Fläche und des Umfangs beobachtet, genauso wie auf der mittleren Ebene der Stent-Ebene (Ebene 3b) und der oberen Ebene der Stent-Ebene (Ebene 4b) im postoperativen CT. Das begradigte Modell wies eine hohe Korrelation mit dem anatomischen Modell auf. Der Pearson-Korrelationskoeffizient zwischen dem begradigten Modell und dem anatomischen Modell für die Querschnittsfläche, den Umfang, den minimalen Durchmesser und den maximalen Durchmesser lag zwischen 0,77 und 0,99 ($P < 0,0001$). Die Grenzen der

Übereinstimmung aus der Bland-Altman-Analyse lagen in einem guten Bereich, was die große Übereinstimmung zwischen dem begradigten Modell und dem anatomischen Modell weiter bestätigt.

Schlussfolgerungen: Das anatomische 4D-CT-Modell kann verwendet werden, um die Verformung der Dynamik zwischen RVOT und PA während des Herzzyklus zu demonstrieren. Das begradigte Modell kann die Veränderungen im Landebereich zeigen, diese Daten genau messen und die Struktur der verschiedenen Abschnitte deutlich darstellen.

1 Introduction

Nearly 20% of neonates with congenital heart disease exhibit complicated defects of the right ventricular outflow tract (RVOT) requiring surgical treatment for RVOT reconstruction from a very young age[1, 2]. Fortunately, the advent of transcatheter pulmonary valve replacement (TPVR) has provided a promising treatment option for this patient population. Since Bonhoeffer et al.[3] performed TPVR in 2000 for the first time, this procedure has become a standard interventional therapy in patients with pulmonary valve dysfunction. Compared with surgical pulmonary valve replacement, the TPVR has merged as a revolutionary treatment with numerous superiorities such as avoidance of complications from cardiopulmonary bypass and median sternotomy[4, 5].

The bioprosthetic valves that are currently widely used in TPVR are mostly from the bovine or porcine tissues, which may potentially deteriorate over time because of the graft versus host reactions[6]. Furthermore, the TPVR valves currently on the market have limited durability because of unfavorable tissue remodeling[7]. These limitations could lead to valve leaflet retraction and valvular dysfunction. As a result, many of these patients are required to undergo valve replacement interventions many times throughout their lifetime, eventually increasing mortality and the rate of surgical complications[8].

To sum up, a new idea was thought out to obtain a long-term durable bioprosthetic pulmonary valve for TPVR. The bioprosthetic pulmonary valve made from patient's autologous pericardium tissue was implanted, which would avoid graft versus host reactions and then prolong the life of the valve.

Currently, it has been found that under the influence of the heart's pumping over the cardiac cycle there has been an increasingly wide knowledge that the RVOT dimensions may vary[9]. Such variation should be taken into account in valve sizing selection before the TPVR. However, the end-diastole has mostly been used in clinical practice for pre-operative assessment, which would inevitably affect the accuracy of RVOT dimension measurement during the entire cardiac cycle. The inaccurate sizing would increase the device-related paravalvular leak (PVL)[10, 11].

With the four-dimension (4D) computed tomography (CT) technique has been increasingly used in medical research, and also in patient-specific therapeutic planning for patients with structural heart valve disease[12, 13]. In some studies, the 4D computed tomography angiography (CTA) has been proven to provide unique view for assessing the dynamic anatomy measurements over the heart cycle in pre- and post-operative transcatheter aortic valve implantation (TAVI)[14-16]. Nonetheless, this technique is rarely used for TPVR procedures. The accurate measurement of the deformation of the landing zone for the implantation site in the TPVR plays an important role in preventing PVL, coronary compression, and migration of bioprosthesis[17]. Thus, in terms of the multi-parameter measurements of RVOT to pulmonary artery (PA) 4D structure, the diameter, area and circumference are particularly important. The traditional 4D segmentation was more focused on the anatomical model reconstruction. A straightening model has not been used to show landing zone deformation. Compared with the conventional anatomical model, the straightened model is more advantageous for showing the structure of the RVOT adjacent to the aortic root.

In the present study, we conducted 4D reconstruction and multiparametric characterization analyses of straightened segmentation from pre- and post-operative CTA for the transcatheter pulmonary valve replacement procedure in sheep. This present study aims to evaluate the feasibility and accuracy of 4D CTA straightened segmentation and simulate the three-dimension (3D) deformation of each section from RVOT to PA throughout the entire cardiac cycle in vivo. In addition, it can identify the benefits of 4D CT straightened model reconstruction for application in TPVR.

2 Materials and Methods

The GrOwnValve preclinical trial (IC14-G 0062/18) was approved by the legal and ethical committee at the Regional Office for Health and Social Affairs, Berlin (LAGeSo). And in full adherence to the European and German Societies of Laboratory Animal Science (FELASA, GV-SOLAS) guidelines. A total of seven adult sheep (Ovis aries) were enrolled in the present study to be conducted transcatheter pulmonary valve replacement with autologous pericardium at Charité University Hospital of Berlin, Campus Virchow-Klinikum, Research Institute for Experimental Medicine. The whole experimental process of the present study is following the flow diagram as shown in Figure 1.

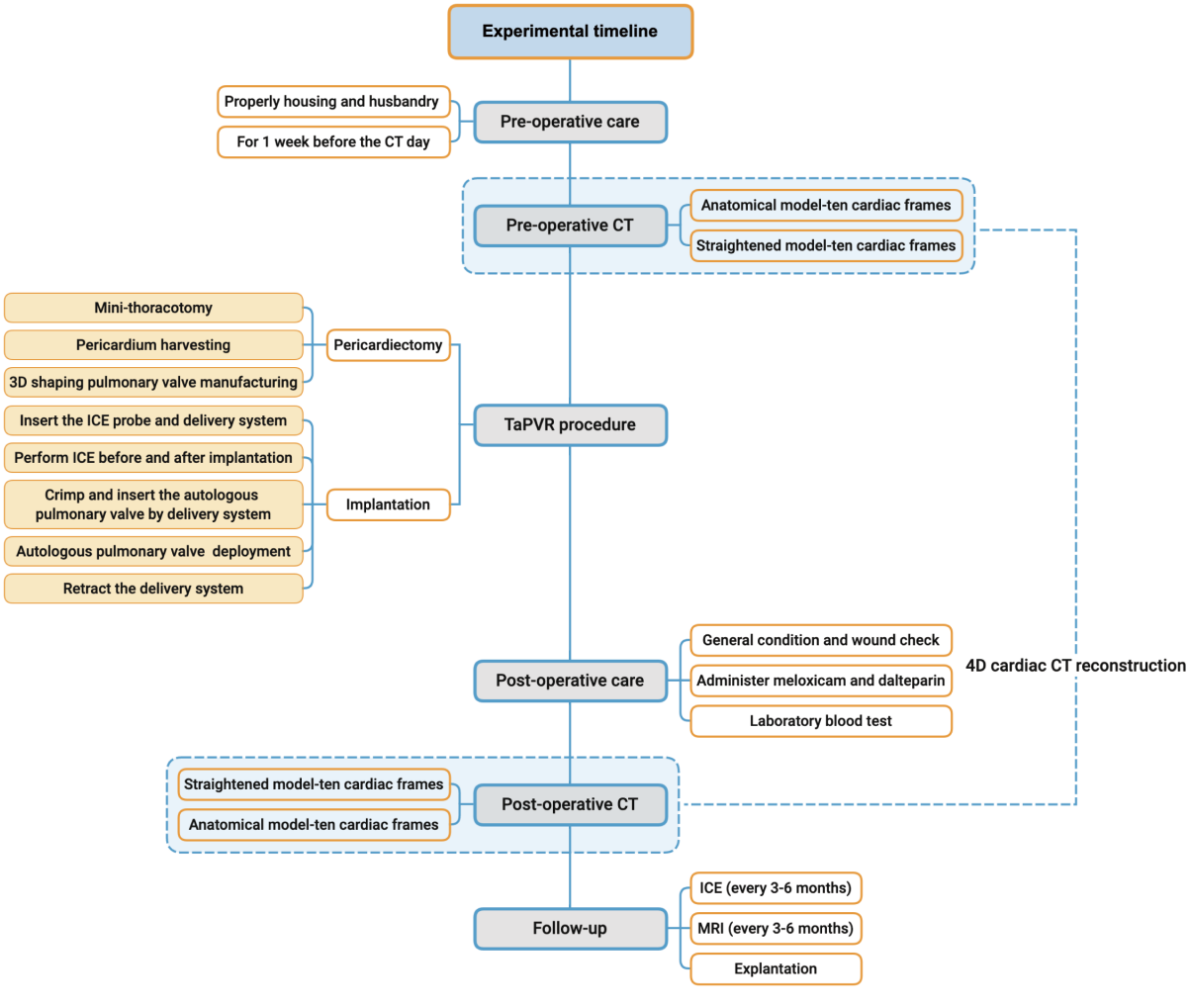

Figure 1. Experimental Flow Diagram. (Own elaboration modified from Hao, Y., Sun, X., Kiekenap, J. F. S., Emeis, J., Steitz, M., Breitenstein-Attach, A., Berger, F., & Schmitt, B. (2022). Transcatheter Pulmonary Valve Replacement from Autologous Pericardium with a Self-Expandable Nitinol Stent in an Adult Sheep Model. *Journal of visualized experiments : JoVE*, (184), 10.3791/63661.)

2.1 4D cardiac CT segmentation

2.1.1 Image acquisition

A Siemens 64-slice dual-source multidetector CT scanner with ECG gating (SOMATOM Definition Flash, Siemens AG, Germany) was used for all CT images. Imaging parameters were as follows: 120 kV tube voltage, 100-320 mAs per rotation, gantry rotation time 0.33 s, matrix 256 with a 16-bit depth. Administer iodinated contrast agent (2-2.5 mL/kg) at a 5 mL/s rate. Each CT was produced into 10 phases between 10 and 100% (10% increments) of the cardiac cycle[18]. All pre- and post-operative CTs were performed at German Heart Center Berlin. The pre-operative CTs were performed 1 week before TPVR, and the post-operative CTs were performed after the implantation during the follow-up before the explanation.

2.1.2 Anatomical segmentation and straightened segmentation

The 4D cardiac CT reconstruction from seven sheep was performed on open-source software 3D Slicer. The detailed 4D segmentation protocol has been described elsewhere[18]. First, the CT dataset was imported into the 3D Slicer (Figure 2A) shown from axial, coronal, and sagittal three directions and use the Segmentation Editor module to create a whole heart segmentation in each single 10% frame (Figure 2B), then a 4D beating heart volume model can be obtained. Second, the left heart system was cut out with the Scissors effect, and the desired structure (from the superior vena cava to right atrium to the right ventricle to the RVOT to the end of the main PA) was kept getting the conventional anatomical model (Figure 2C). Last, the straightening model was established with the corresponding anatomical model. The Extract Centerline module was used to create a new curve as the centerline curve from the superior vena cava to the main PA throughout the anatomical model. Then we can select the Curved Planar Reformat module to create a straightened model (Figure 2D). By repeating this procedure every 10% of frames over the entire cardiac cycle, we can obtain a complete 4D cardiac CT straightened segmentation.

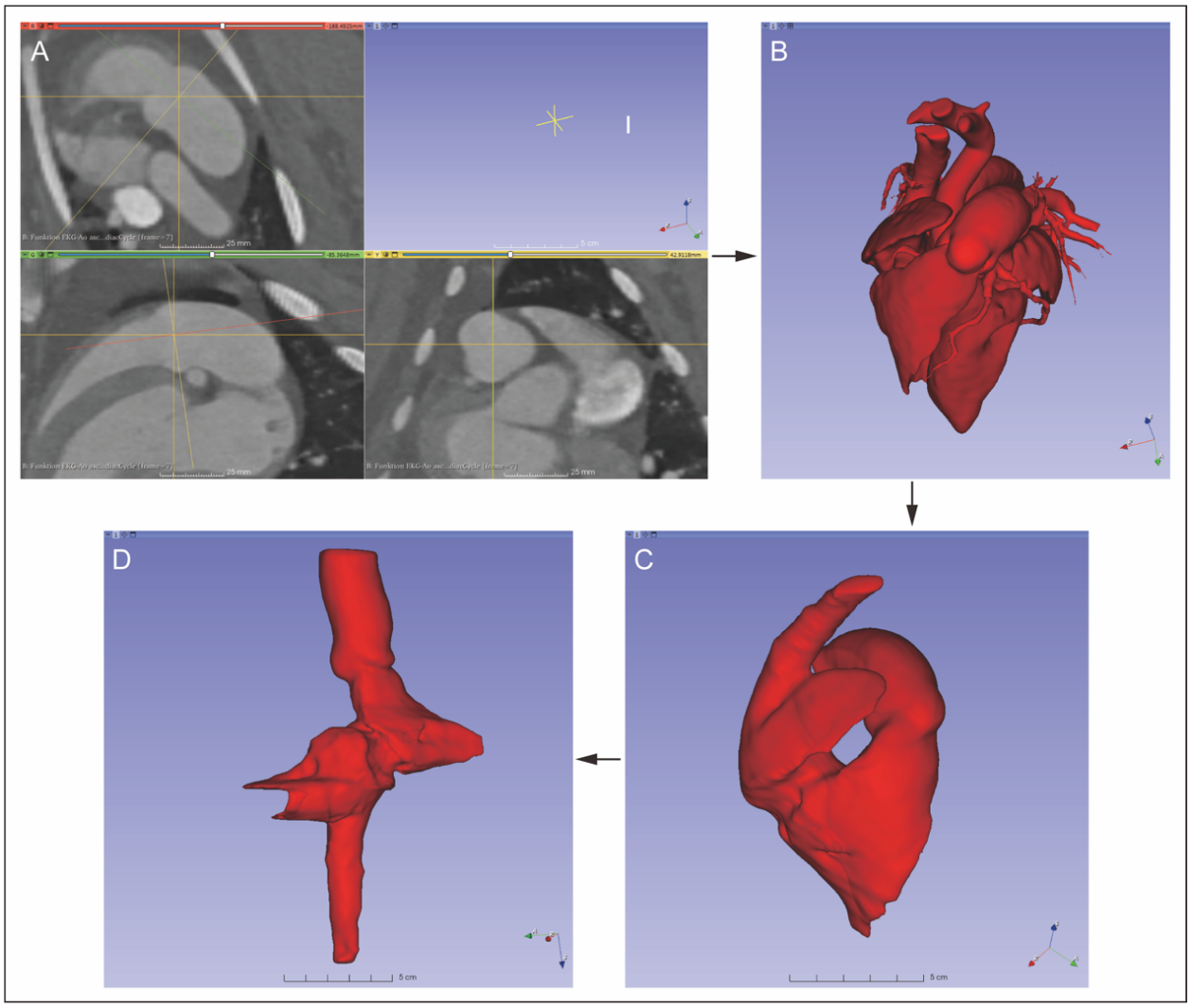

Figure 2. One description of the procedure for 4D cardiac CT reconstruction. (Own elaboration modified from Sun, X., Hao, Y., Sebastian Kiekenap, J. F., Emeis, J., Steitz, M., Breitenstein-Attach, A., Berger, F., & Schmitt, B. (2022). Four-Dimensional Computed Tomography-Guided Valve Sizing for Transcatheter Pulmonary Valve Replacement. *Journal of visualized experiments : JoVE*, (179), 10.3791/63367.)

(A) The interface of 3D Slicer software. The CTA images were shown from three directions (axial, coronal, and sagittal). (B) One frame of whole heart model created by Segmentation Editor module. (C) One frame of the right heart conventional anatomical model. (D) One frame of the right heart straightened model created from corresponding anatomical model.

2.2 Multiparametric measurements of the landing zone

The landing zone for transcatheter pulmonary valve deployment were defined from the RVOT to the PA. For pre-operative CT, each landing zone was characterized at five selected landmarks:

Plane 1a: The right ventricular outflow tract level (10mm below Plane 2a)

Plane 2a: The basal plane of the pulmonary valve, the three hinge points at the end of each attachment of the pulmonary valve
Plane 3a: The valvular sinuses level
Plane 4a: The sino-tubular junction plane
Plane 5a: The PA level, 10 mm above the Plane 4
For post-operative CT, the five selected landmarks were as following:
Plane 1b: The RVOT plane (10mm below Plane 2b)
Plane 2b: The bottom plane of the stent level
Plane 3b: The middle plane of the stent level
Plane 4b: The top plane of the stent level
Plane 5b: The PA plane, 10 mm above the Plane 4b

The multi-parametric characteristic measurements include the cross-sectional area (mm^2), circumference (mm), minimum diameter (mm), and maximum diameter (mm) at each selected plane in every 10% of the cardiac phase. Then the mean value of the cross-sectional area and circumference at each plane were calculated to present the dynamic variation trend during the entire cardiac cycle. We also calculated the ellipticity index by the ratio between the minimum diameter and maximum diameter to show the shape changes of the conduit from the RVOT to the PA. Furthermore, the correlation and agreement between the anatomical model and straightened model were assessed to confirm the accuracy of the straightened model. Apart from these parameters, the right ventricular volume to get the right ventricular ejection fraction, stent volume, as well as the relationship between the stented PA and left coronary artery from the 4D CT reconstruction model were measured.

2.3 TPVR procedure

2.3.1 Preoperative care and anesthesia

All the sheep got proper housing and husbandry for the whole experiment from arrival to the sacrifice day. The whole procedure (pericardiectomy and implantation) was performed under general anesthesia. Twenty minutes before anesthesia induction, the sheep were administered with pre-medication, which consisted of midazolam (0.4 mg/kg), butorphanol (0.4 mg/kg), and glycopyrrolate 0.011 mg/kg by intramuscular injection, so that the sheep could cooperate more easily. After the sheep become docile, administer

the anesthesia induction by intravenous injection of propofol 1-2.5 mg/kg and fentanyl 0.01 mg/kg. Then the sheep were intubated and maintained general anesthesia with isoflurane (1-1.5%) combined with a continuous rate intravenous infusion of fentanyl (5-15 mcg/kg/h) and midazolam (0.2-0.5 mg/kg/h) during the procedure. Furthermore, the hemodynamics, internal environment of the experimental sheep, and fluid management were administered according to the intraoperative situation.

2.3.2 Mini-thoracotomy and pericardiectomy

After the general anesthesia induction and intubation were finished, the sheep was immobilized in the right lateral recumbent position with a 30-degree elevation on the operating table. After the disinfection and draping completion, under the guidance of an ultrasound probe, a 5 cm incision was created in the third and fourth intercostal space for the mini thoracotomy. Then a rib spreader was placed to open the thorax for a clear view of the heart. The excess tissue was resected to expose the pericardium, then the pericardium was cut from the pericardium-diaphragm attachment point and the cut extended upwards to the lateral wall of the ventricle and atrium to extract the pericardium (between the two phrenic nerves, up to the innominate veins, down to the diaphragm, about 9×9 cm). In the end, staunch any bleeding from the incision and suture the muscles and skin. Asepsis gauze was then used to cover the incision and compress it for five minutes. After harvesting the autologous pericardium, we transferred the pericardium into 0.9% NaCl and rinse twice to keep it moist. While trimming the pericardium to remove any adipose tissue before placing it onto the 3D shaping heart valve mold for crosslinking, then suture the crosslinked heart valve onto a nitinol stent to manufacture the autologous pulmonary valve.

2.3.3 Implantation

After obtaining the autologous pulmonary valve, the implantation area was disinfected and the sheep was covered with sterile draping but the surgical area was expose. Then, the intra-cardiac echocardiography (ICE) probe was insert into the left jugular vein for performing the ICE before the implantation to assess the dimensions and functions of the pulmonary valve. During the whole implantation procedure, the right ventricle and pulmonary angiography were performed to double-check the diameters of the conduit from RVOT to supravalvular PA. The autologous pulmonary valve was re-crimped and inserted into the head of the delivery system. The loaded delivery system was then

advanced to the native pulmonary valve location guided by the pre-shaped guidewire. Then angiography was carried out for the sake of ensuring that the stent-bearing portion of the delivery system is in the desired position and deploying the autologous pulmonary valve over the native pulmonary valve under the guidance of fluoroscopy. After the deployment, the delivery system was withdrawn. In the end, angiography and ICE were repeated for a post-examination of the dimensions and functions of the implanted autologous pulmonary valve.

2.3.4 Post-operative care and follow-up

After the implantation, daily post-operative care was performed on the following five days, including, checking the experimental sheep's general condition in terms of breathing, heartbeat, signs of pain, and the wound for postoperative swelling, redness, secretion, bleeding, and overheating. The subjects were administered with Meloxicam (0.5 mg/kg, SC) for postoperative analgesia and Dalteparin (5000 IU/d, SC) for anticoagulation for five days.

During the follow-up period, the final cardiac CT was performed the same as the pre-operative CT to evaluate the position and the deformation of the implanted stent. ICE and cardiac magnetic resonance imaging (cMRI) were performed every 3-6 months after TPVR for up to about one year to evaluate the regurgitation fraction of the implanted autologous pulmonary valve as well as the PA pressure and right ventricular pressure.

2.4 Statistical analysis

A Kolmogorov–Smirnov test was used to assess the normal distribution. The continuous data were summarized as mean ± standard deviation (SD) for normal distribution or as median with interquartile ranges (IQRs) for non-normal distribution. The linear correlation between each plane of the conventional anatomical model and straightened model was quantitatively assessed by the Pearson correlation coefficient. The bias and agreement between the two models were further confirmed by the Bland-Altman analysis. A paired t-test was used to quantify the significance of differences in cross-sectional area and circumference at five planes between each 10% of the cardiac cycle phases. Matrices were generated to indicate the t-test result. The differences were considered statistically

significant if p-values of 0.05 or less. All the statistical analyses were performed using the GraphPad Prism 9 software.

3 Results

3.1 4D cardiac CT segmentation

Seven sheep were successfully performed the TPVR procedure including mini-thoracotomy, pericardiectomy, and autologous pulmonary valve implantation and conducted about 1-year follow-up. Throughout the above procedure, we obtained one pre-operative CT and one post-operative CT from each sheep. It means a total of 14 cardiac CT datasets were included in the study. In addition, each cardiac CT was divided into ten phases of the cardiac cycle. The representative example of reconstructed anatomical model and straightened model with selected planes of landing zone for pre- and post-operative CT were shown in Figure 3, 4.

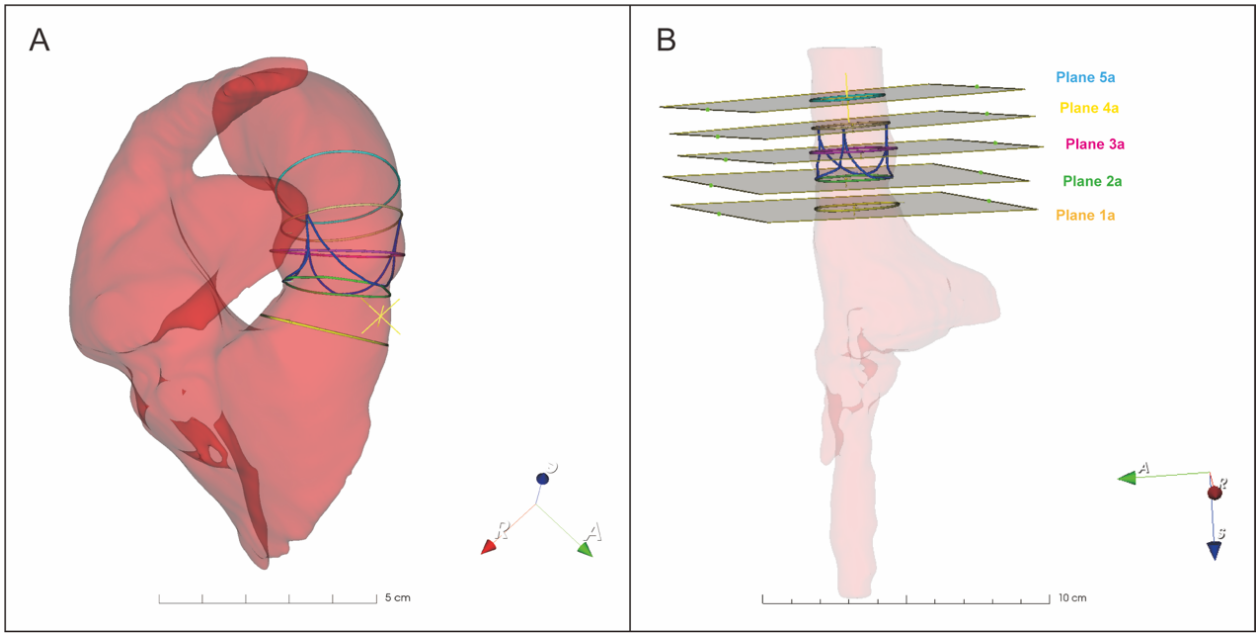

Figure 3. The anatomical model and straightened model with selected planes of landing zone for pre-operative CT. (Own elaboration modified from Sun, X.; Hao, Y.; Steitz, M.; Breitenstein-Attach, A.; Kiekenap, J. F. S.; Emeis, J.; Khan, M. B.; Berger, F.; Schmitt, B., Straightened Segmentation in 4D Cardiac CT: A Practical Method for Multiparametric Characterization of the Landing Zone for Transcatheter Pulmonary Valve Replacement. *Applied Sciences* 2022, *12* (24).)
(A) The five selected planes for pre-operative CT of anatomical model. (B) The five selected planes for pre-operative CT of straightened model. *Turquoise* loop of the Plane 5a, *light yellow* loop of the Plane 4a, *fuchsia red* loop of the Plane 3a, *green* loop of the Plane 2a, *deep yellow* loop of the Plane 1a, *royal blue* hinges of the pulmonary valve.

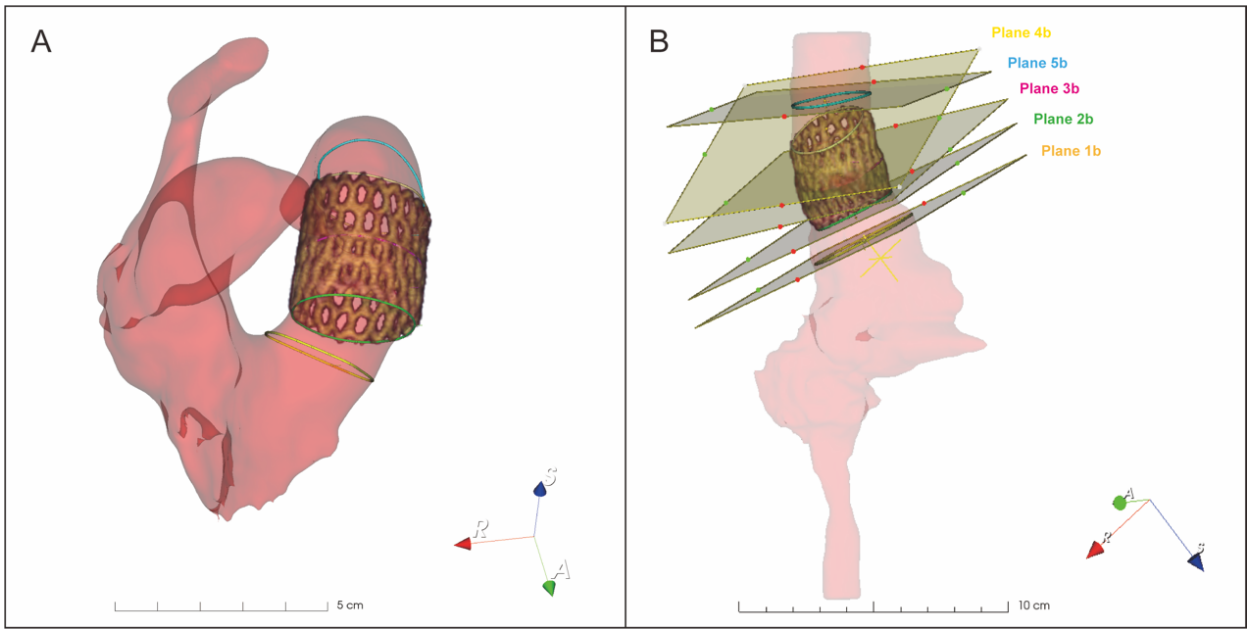

Figure 4. The anatomical model and straightened model with selected planes of landing zone for post-operative CT. (Own elaboration modified from Sun, X.; Hao, Y.; Steitz, M.; Breitenstein-Attach, A.; Kiekenap, J. F. S.; Emeis, J.; Khan, M. B.; Berger, F.; Schmitt, B., Straightened Segmentation in 4D Cardiac CT: A Practical Method for Multiparametric Characterization of the Landing Zone for Transcatheter Pulmonary Valve Replacement. *Applied Sciences* 2022, *12* (24).)
(A) The five selected planes for post-operative CT of anatomical model. (B) The five selected planes for post-operative CT of straightened model. *Turquoise* loop of the Plane 5b, *light yellow* loop of the Plane 4b, *fuchsia red* loop of the Plane 3b, *green* loop of the Plane 2b, *deep yellow* loop of the Plane 1b.

3.2 Multiparametric measurements of the landing zone

3.2.1 Correlations between anatomical model and straightened model

Each CT was reconstructed into an anatomical model and a straightened model in the present study. A total of 28 models including 14 anatomical models and 14 straightened models were successfully reconstructed. Each model was consisting of ten cardiac phases. The selected landmarks from the landing zone were defined in all 28 models. The correlation analyses between the conventional anatomical model and straightened model of seven sheep were conducted separately in pre- and post-operative CT. Finally, the parameters (cross-sectional area, circumference, minimum diameter, and maximum diameter) were measured at each selected plane for all seven sheep, with 70 paired data in each comparison.

A statistically significant linear correlation was observed between the conventional anatomical model and straightened model for cross-sectional area measurements at

planes 1a, 2a, 3a, 4a, and 5a of pre-operative CT with the Pearson correlation coefficient of 0.96, 0.87, 0.93, 0.97, and 0.97, respectively ($P < 0.0001$). In addition, the Pearson correlation coefficient between the two models for circumference from pre-operative CT was highly correlated. The r values for five planes of landing zone were 0.95 for Plane 1a, 0.84 for Plane 2a, 0.94 for Plane 3a, 0.97 for Plane 4a, and 0.97 for Plane 5a ($P < 0.0001$). The same went to the minimum diameter and maximum diameter. As for minimum diameter, the r values for five planes of landing zone were 0.94 for Plane 1a, 0.88 for Plane 2a, 0.92 for Plane 3a, 0.93 for Plane 4a, and 0.95 for Plane 5a ($P < 0.0001$). As for maximum diameter, the r values for five planes of landing zone were 0.94 for Plane 1a, 0.77 for Plane 2a, 0.90 for Plane 3a, 0.94 for Plane 4a, and 0.92 for Plane 5a ($P < 0.0001$). The scatter plots of Bland-Altman analysis for cross-sectional area, circumference, minimum diameter, and maximum diameter at each plane from pre-operative CT further confirmed a high agreement between the anatomical model and straightened model. The limits of agreement were in a good range for all the planes.

In terms of post-operative CT, a strong correlation with statistically significant linear correlation was observed in the cross-sectional area of the two models at planes 1b, 2b, 3b, 4b, and 5b. The Pearson correlation coefficients were significant between the measurements of the anatomical model and straightened model, with the r values of 0.97, 0.95, 0.99, 0.97, and 0.97, respectively ($P < 0.0001$). A similar result was shown for circumference measurement, the Pearson correlation coefficients of the comparison were 0.97 for Plane 1b, 0.95 for Pla ne 2b, 0.99 for Plane 3b, 0.97 for Plane 4b, and 0.97 for Plane 5b ($P < 0.0001$). The same went to the minimum diameter and maximum diameter. As for minimum diameter, the r values for five planes of landing zone were 0.91 for Plane 1b, 0.84 for Plane 2b, 0.92 for Plane 3b, 0.93 for Plane 4b, and 0.92 for Plane 5b ($P < 0.0001$). As for maximum diameter, the r values for five planes of landing zone were 0.93 for Plane 1b, 0.93 for Plane 2b, 0.96 for Plane 3b, 0.97 for Plane 4b, and 0.94 for Plane 5b ($P < 0.0001$). The Bland-Altman plots showed a high degree of agreement between the anatomical model and straightened model measurements of cross-sectional area, circumference, minimum diameter, and maximum diameter at five selected planes according to post-operative CT.

3.2.2 Dynamic variation of landing zone measurements

The mean value of cross-sectional area and circumference were calculated at all five selected planes in each 10% phase throughout the entire cardiac cycle from the straightened model. The t-test was also conducted to assess the statistically significant differences of all comparisons between each 10% cardiac cycle phase then visually indicated by *P*-value matrices. The mean values of cross-sectional area variations in the corresponding planes during the cardiac cycle are shown in Figure 5, 7. The *P*-value matrices of the t-test result of each plane are shown in Figure 6, 8.

According to the pre-operative CT, a high variation in cross-sectional area was observed at Plane 1a during the cardiac cycle (Figure 5). The area differed highest between 90% and 50% with areas of 646 ± 149 mm² (maximum mean) and 272 ± 122 mm² (minimum mean) ($P < 0.0001$), respectively (Figure 6A). Compared with Plane 1a, the variation of cross-sectional area at the 2a and 5a planes was lower. The maximum area was 471 ± 48 mm² (100%) and the minimum area was 266 ± 101 mm² (60%) at Plane 2a ($P < 0.0001$) (Figure 6B). And the maximum and minimum cross-sectional area of the 5a plane were 582 ± 102 mm² (20%) and 495 ± 88 mm² (100%) ($P = 0.0034$), respectively (Figure 6E). With respect to planes 3a and 4a, almost no significant differences were shown between the combinations during the cardiac cycle shown from the t-test matrices (Figure 6C, 6D).

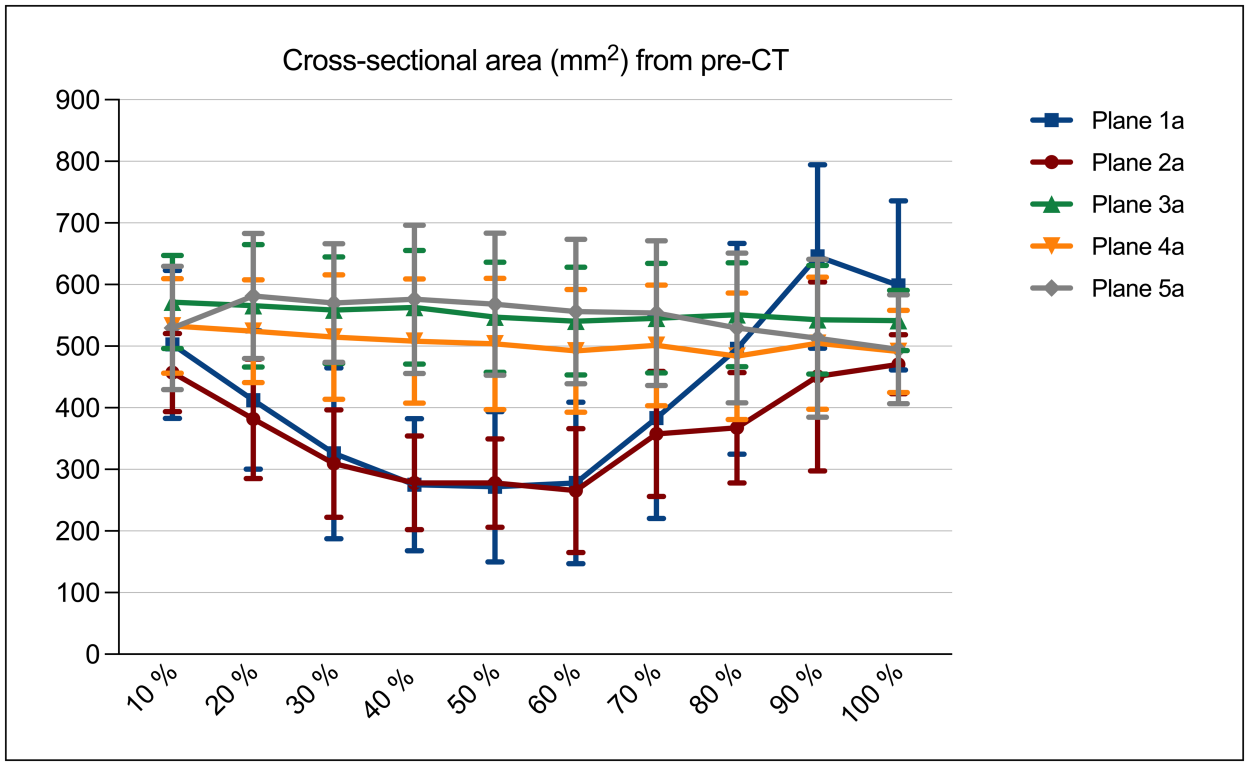

Figure 5. The mean values of cross-sectional area variations in the corresponding planes during the 10 frames of cardiac cycle from pre-operative CT. (Own elaboration modified from Sun, X.; Hao, Y.; Steitz, M.; Breitenstein-Attach, A.; Kiekenap, J. F. S.; Emeis, J.; Khan, M. B.; Berger, F.; Schmitt, B., Straightened Segmentation in 4D Cardiac CT: A Practical Method for Multiparametric Characterization of the Landing Zone for Transcatheter Pulmonary Valve Replacement. *Applied Sciences* 2022, *12* (24).)

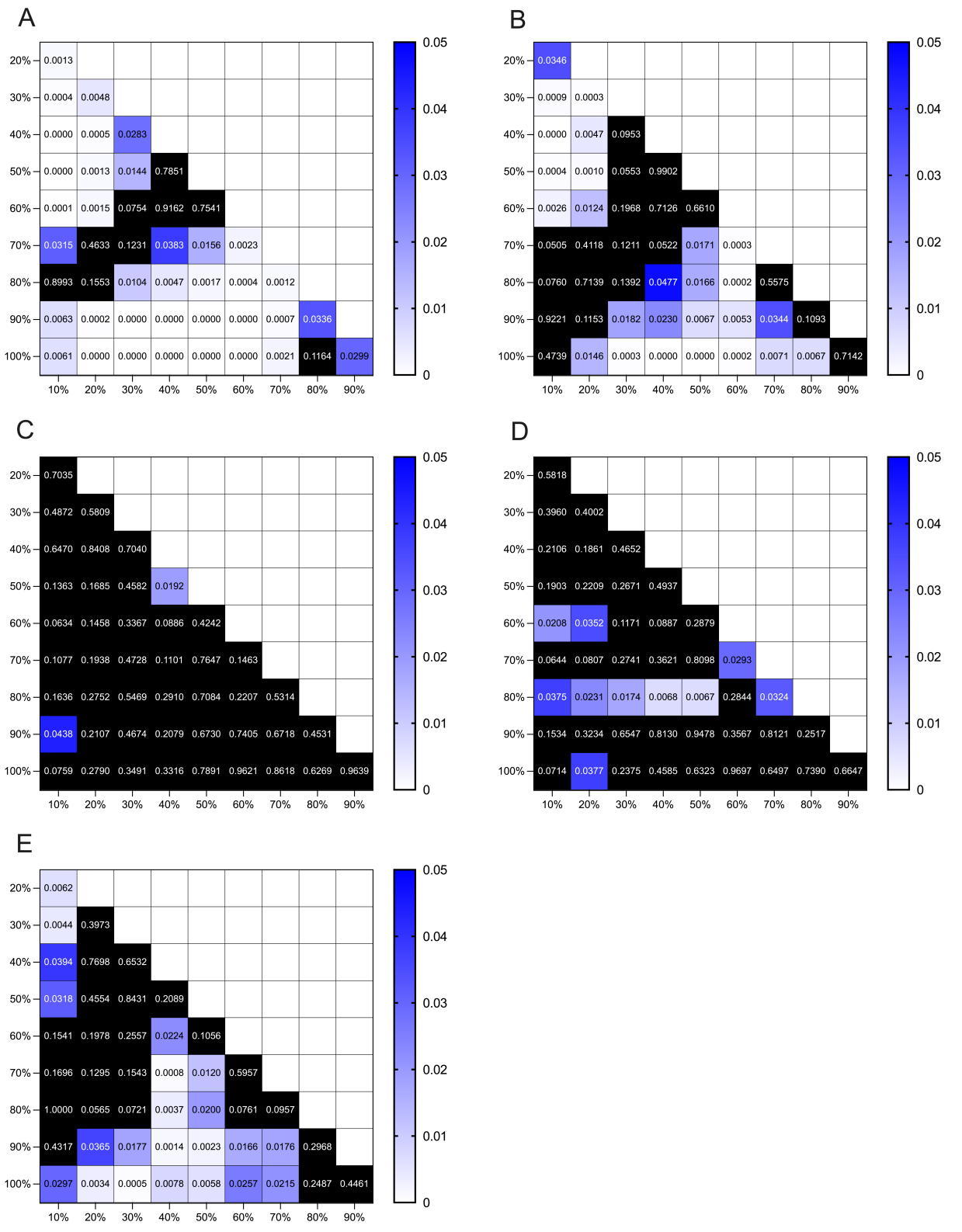

Figure 6. The t-test P-value matrices demonstrating the statistically difference between combinations of each cardiac cycle phases for cross-sectional area at five planes from pre-operative CT. (Own elaboration modified from Sun, X.; Hao, Y.; Steitz, M.; Breitenstein-Attach, A.; Kiekenap, J. F. S.; Emeis, J.; Khan, M. B.; Berger, F.; Schmitt, B., Straightened Segmentation in 4D Cardiac CT: A Practical

Method for Multiparametric Characterization of the Landing Zone for Transcatheter Pulmonary Valve Replacement. *Applied Sciences* 2022, *12* (24).)
(A) *P*-value matrices for Plane 1a. (B) *P*-value matrices for Plane 2a. (C) *P*-value matrices for Plane 3a. (D) *P*-value matrices for Plane 4a. (E) *P*-value matrices for Plane 5a.

For the post-operative CT, same variation trends as pre-operative CT, Plane 1b shows a significantly higher variation among cardiac cycle. The maximum mean and SD for area was 1,028 ± 210 mm² at 100% of the cardiac cycle phase; the minimum mean value was 435 ± 144 mm² at 50% of the phase (P = 0.0003) (Figure 8A). As shown in Figure 7, a lower degree of variation detected was measured at planes 2b and 5b compared to Plane 1b. The differences between the mean maximum and minimum cross-sectional area at planes 2b and 5b were statistically significant with p-values of 0.0137 and 0.0131, respectively (Figure 8B, 8E). Furthermore, the t-test matrices indicated that the differences between each 10% of the cardiac cycle phase at planes 3b and 4b were not statistically significant with a p-value of more than 0.05 (Figure 8C, 8D). The stent radial force for fixing the implanted stent on the vascular wall from the bottom plane to the top plane of the stent levels has led to the vessel expanding fully. Therefore, the variations of the Plane 2b, 3b, and 4b were small. The muscle contraction by RVOT, however, allowed Plane 2b have a higher deformation than the other two. In addition, due to the implanted stent radial force, the Plane 1a and 1b showed a lower ellipticity index (Plane 1a: 0.55 ± 0.08 for pre-operative CT; Plane 1b: 0.69 ± 0.10 for post-operative CT) than other planes (Plane 2a: 0.69 ± 0.12, Plane 3a: 0.89 ± 0.06, Plane 4a: 0.90 ± 0.06, and Plane 5a: 0.83 ± 0.06 for pre-operative CT; Plane 2b: 0.88 ± 0.08, Plane 3b: 0.88 ± 0.09, Plane 4b: 0.84 ± 0.10, and Plane 5b: 0.86 ± 0.09 for post-operative CT), both for pre- and post-operative CTs.

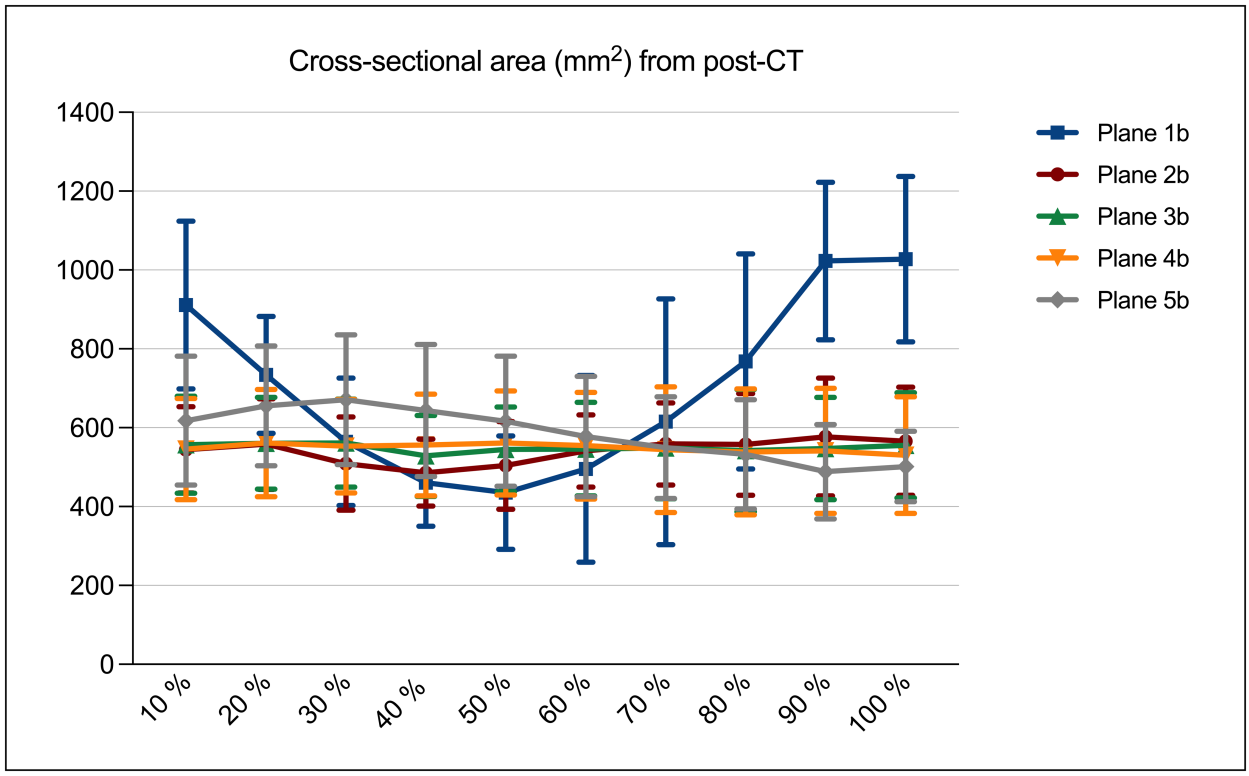

Figure 7. The mean values of cross-sectional area variations in the corresponding planes during the 10 frames of cardiac cycle from post-operative CT. (Own elaboration modified from Sun, X.; Hao, Y.; Steitz, M.; Breitenstein-Attach, A.; Kiekenap, J. F. S.; Emeis, J.; Khan, M. B.; Berger, F.; Schmitt, B., Straightened Segmentation in 4D Cardiac CT: A Practical Method for Multiparametric Characterization of the Landing Zone for Transcatheter Pulmonary Valve Replacement. *Applied Sciences* 2022, *12* (24).)

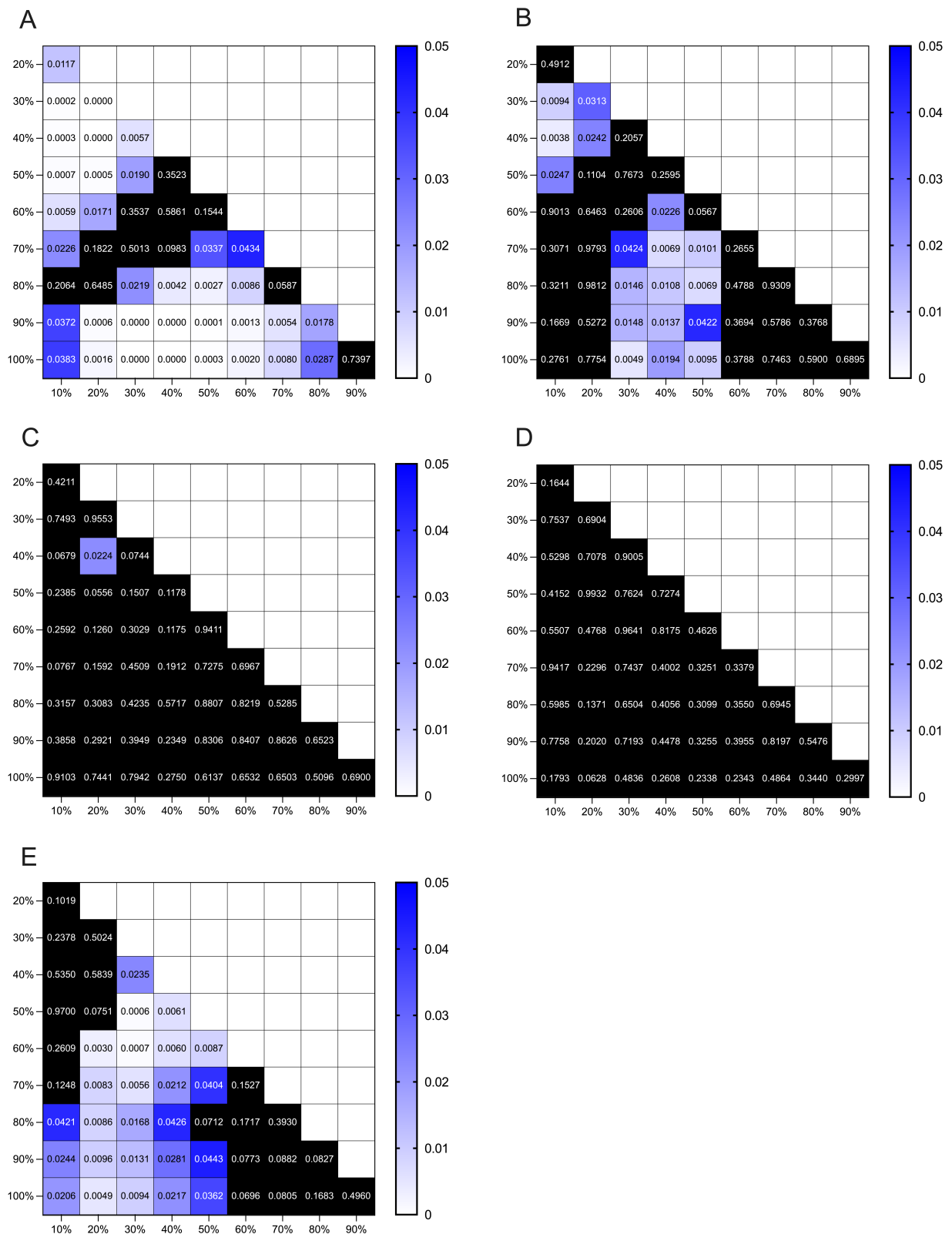

Figure 8. The t-test P-value matrices demonstrating the statistically difference between combinations of each cardiac cycle phases for cross-sectional area at five planes from post-operative CT. (Own elaboration modified from Sun, X.; Hao, Y.; Steitz, M.; Breitenstein-Attach, A.; Kiekenap, J. F. S.; Emeis, J.; Khan, M. B.; Berger, F.; Schmitt, B., Straightened Segmentation in 4D Cardiac CT: A Practical

Method for Multiparametric Characterization of the Landing Zone for Transcatheter Pulmonary Valve Replacement. *Applied Sciences* 2022, *12* (24).)
(A) *P*-value matrices for Plane 1b. (B) *P*-value matrices for Plane 2b. (C) *P*-value matrices for Plane 3b. (D) *P*-value matrices for Plane 4b. (E) *P*-value matrices for Plane 5b.

The circumference dynamic variation trends were similar to the cross-sectional area where Plane 1a and 1b showed the highest variation behavior than other planes.

3.3 The outcomes of the TPVR

TPVR procedure has been successfully conducted for all these seven sheep. The result showed that none of them had procedure-related complications. The regurgitation fraction of implanted autologous pulmonary valve of seven sheep obtained from the follow-up MRI was ranged from 5.6% to 57%, and the mean value was 30.23 ± 21.15 %. The PA pressure was measured by the follow-up ICE, of which, the systolic pressure was ranged from 19 to 31 mmHg (mean: 23.43 ± 3.74 mmHg), and the diastolic pressure was ranged from 6 to 14 mmHg (mean: 10.29 ± 3.04 mmHg). The right ventricular pressure measured from the follow-up ICE, of which, the systolic pressure was ranged from 23 to 37 mmHg (mean: 28.00 ± 4.51 mmHg), and the diastolic pressure was ranged from 0 to 14 mmHg (mean: 3.71 ± 5.06 mmHg).

In addition, the right ventricular volume and stent volume were obtained from the right heart segmentation of the 4D post-operative CT straightened model. Right ventricular ejection fraction was further obtained from the right ventricular volume, ranging from 43.1% to 73.5% with the mean ± SD of 62.92 ± 10.4 %. The calculated stent volumes vary in each 10 frames of the cardiac cycle. The maximum and minimum values were 20.09 ± 3.74 mm^3 and 17.99 ± 3.42 mm^3, respectively. Besides, the anatomical relationship between the stent and the coronary artery has been clearly observed from post-operative 4D CT. The stent was deployed and anchored in the target location without any compression of the left circumflex artery and left anterior descending artery (Figure 9).

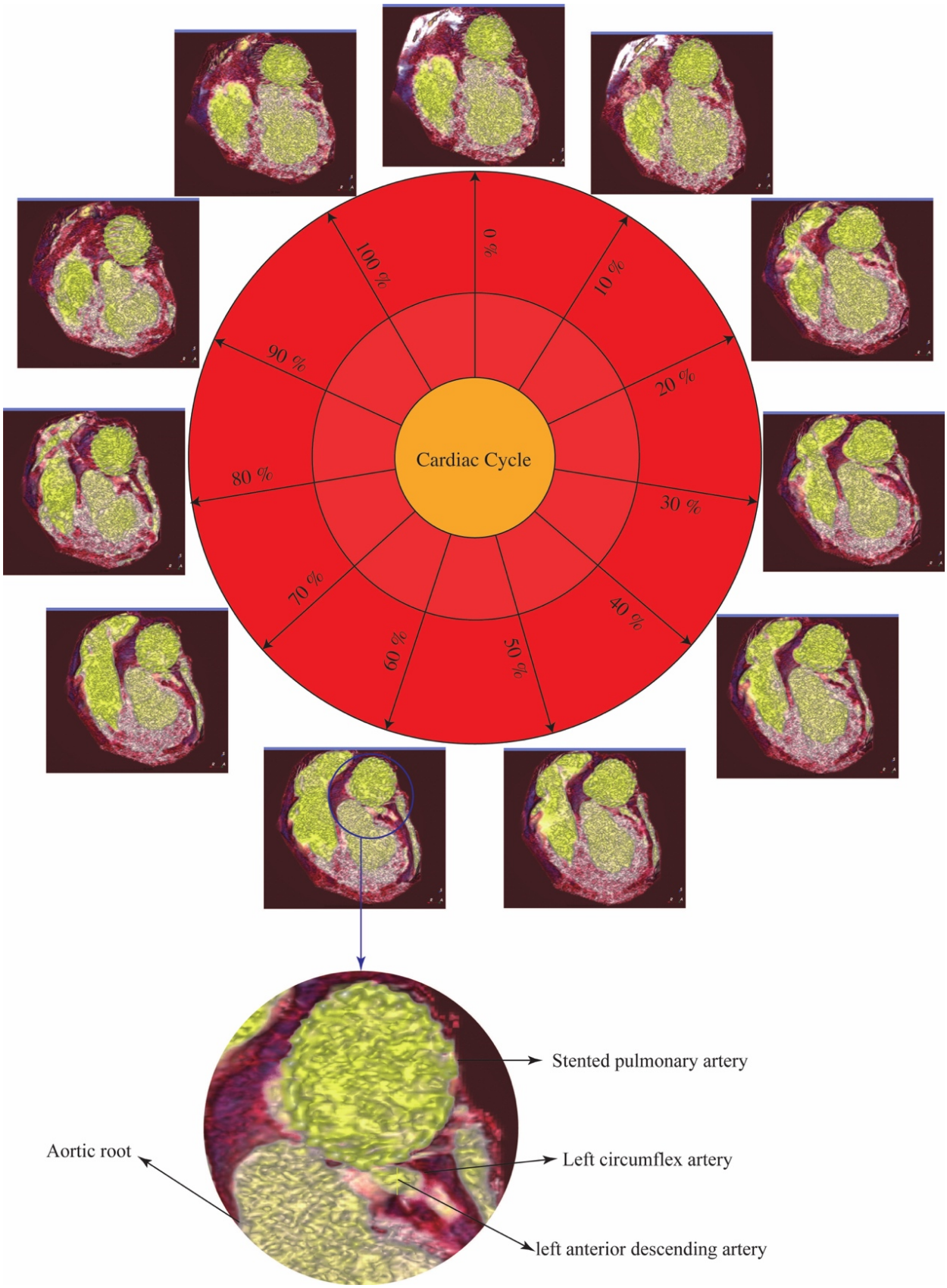

Figure 9. One representative example of the relationship between the stented pulmonary artery and left coronary artery. (Cited from Hao, Y., Sun, X., Kiekenap, J. F. S., Emeis, J., Steitz, M., Breitenstein-Attach, A., Berger, F., & Schmitt, B. (2022). Transcatheter Pulmonary Valve Replacement from Autologous Pericardium with a

Self-Expandable Nitinol Stent in an Adult Sheep Model. ***Journal of visualized experiments : JoVE*****, (184), 10.3791/63661**[19]**)**
The stent was deployed and anchored in the target location without any compression of the left coronary artery.

4 Discussion

4.1 Importance of accurate landing zone assessment

Standard 2D and 3D echocardiography, MRI, and CT enable to assessment of the deformation and contraction movement of the myocardial, but the evaluation of RVOT to PA strains and displacement is still inadequate[20, 21]. However, the morphology of the landing zone is crucial to the pre-operative assessment for patients requiring transcatheter heart valve replacement[22]. In terms of patients with congenital structural heart disease, several times of surgeries might change the anatomical structures of RVOT and PA, which may increase the difficulty of accurate valve size evaluation[23, 24]. These patient populations that require secondary TPVR should take even more significant consideration on that score. Inadequate valve sizing selection will increase the risk of post-operative valvular regurgitation, paravalvular leak, and stent fracture leading to a poor performance of implanted heart valve and stent[25-27].

In the present study, therefore, we conducted the 4D conventional right heart anatomical model and straightened model reconstruction from CTA instead of 2D or 3D images. We also selected five different planes through RVOT to the main PA of the landing zone from the pre- and post-operative cardiac CT. The multiparametric measurements, including cross-sectional area, circumference, and diameter at each plane of the landing zone in the pre- and post-operative CT were performed on the straightened model to show the landing zone dynamic variation at each plane from RVOT to PA, and the shortening and stretching of the vessel wall throughout the whole cardiac cycle, which could be used for accurate multiparametric pre-operative evaluation in clinical practice for the TPVR patients.

On the other hand, the implanted stent position and morphology are also vital for the post-operative evaluation. Much attention has been paid to right ventricular and new valve function in patients after TPVR. In contrast, the morphology of the implanted stent has been least concerned. In this study, the multiparametric measurements were performed for the function of the right ventricle and implanted stent evaluation in the post-operative 4D segmentation as well.

4.2 The variation of landing zone

In addition to the measurements of cross-sectional area and circumference, the ellipticity ratio at each plane was calculated by the ratio between the minimum diameter and maximum diameter for the sake of reflecting the elliptical geometry of the cross-sections. The result showed a more notable elliptical geometry at the RVOT and the basal plane of the pulmonary valve than other planes in pre-operative CT, while only the RVOT plane was observed in post-operative CT due to the radial force of the stent[28]. The changes in the ellipsoid annulus would be an application for future TPVR device design. As reported in the study by Schymik G, et al., the elliptical geometry form plays an important role in pre-sence for transcatheter heart valve replacement to avoid the PVL[29].

The measurement of the landing zone at the end-diastolic phase has been mostly taken into account for the pre-operative assessment in the previous studies[25]. Nonetheless, according to the calculated mean values of cross-sectional area and circumference at each plane over the 10 frames of the cardiac cycle in the present study, there were the largest dimension measurements at the basal plane of the pulmonary valve and the sino-tubular junction plane during the mid-systolic phase. Thus, it would be better to select valve size according to the parameters of more phases.

4.3 The advantages and accuracy of straightened model

In the study by Bruns S, et al., cardiac CT was developed into whole-heart 4D segmentation for TAVI procedure in clinical practice. The high feasibility of the 4D segmentation from cardiac CT has been determined[30]. Current studies about 4D cardiac CT reconstruction are all on the basis of the anatomical model and the accuracy of anatomical segmentation in cardiology has been confirmed[10, 12, 13]. Nevertheless, the conventional anatomical segmentation is not able to show the structure of the RVOT adjacent to the aortic root clearly due to the overlap of these two structures reflected in the anatomical model. In the present study, a method of reconstructing the straightened model was used based on the right heart model to stretch out the curved overlap structure to get an excellent visualization of the landing zone. In future clinical practice, therefore, the straightened right heart visual images from 4D segmentation could show the dynamic deformation trends of the elliptical cross-section through axial, coronal, and sagittal directions from the superior vena cava to the right atrium to the right ventricle to the RVOT

to the end of the main PA without any overlapping structures. However, the accuracy of the straightened model has never been evaluated in previous studies. In the present study, therefore, the feasibility and accuracy of the 4D straightened segmentation by the linear correlation and agreement analysis between the anatomical model and straightened model was performed. According to the results of the correlation analysis, a significant linear relationship of dimension measurements between the anatomical model and straightened model has been confirmed, as reflected by the high correlation coefficients. Besides, the Bland-Altman analysis certified the accuracy of straightened reconstruction model in the present study.

5 Limitations

There are several limitations that must be acknowledged in the present study. First, the results need to be further confirmed by a larger sample study as the number of sheep used to analyze the feasibility and accuracy of the straightened models for multiparametric dimensions measurements. Second, the cardiac cycle was only divided into 10 frames. Hence, in the future study, the cardiac cycle needs to be divided into more and shorter frames for obtaining a more accurate and coherent 4D model. Finally, all the CT datasets were obtained from healthy sheep without anatomical structure changes in the present study. In terms of clinical practice, it is inadequate for patients with congenital heart disease.

6 Conclusions

To sum up, as a conclusion, 4D straightened segmentation- that can perform the multiparametric characterization analysis for TPVR. Compared with 3D imaging, the 4D CT segmentation can be used to demonstrate the deformation of RVOT to PA dynamics over the cardiac cycle. In addition, compared with the anatomical model, the straightened model is able to show the landing zone variation for accurate measurements and the clear structure of each section in a better manner. Plus, this method can provide patient-specific planning for the pre- and post-operative assessment for the TPVR clinical practice. Furthermore, the right ventricular volume can be successfully obtained by this methodology, then calculate the right ventricular ejection fraction, which may aid in the understanding of in vivo right ventricular function.

7 Bibilography

1. Georgiev, S.; Ewert, P.; Eicken, A.; Hager, A.; Hörer, J.; Cleuziou, J.; Meierhofer, C.; Tanase, D., Munich Comparative Study: Prospective Long-Term Outcome of the Transcatheter Melody Valve Versus Surgical Pulmonary Bioprosthesis With Up to 12 Years of Follow-Up. *Circ Cardiovasc Interv* **2020,** *13* (7), e008963.
2. Yuan, S. M.; Mishaly, D.; Shinfeld, A.; Raanani, E., Right ventricular outflow tract reconstruction: valved conduit of choice and clinical outcomes. *J Cardiovasc Med (Hagerstown)* **2008,** *9* (4), 327-37.
3. Bonhoeffer, P.; Boudjemline, Y.; Saliba, Z.; Merckx, J.; Aggoun, Y.; Bonnet, D.; Acar, P.; Le Bidois, J.; Sidi, D.; Kachaner, J., Percutaneous replacement of pulmonary valve in a right-ventricle to pulmonary-artery prosthetic conduit with valve dysfunction. *Lancet* **2000,** *356* (9239), 1403-5.
4. Kheiwa, A.; Divanji, P.; Mahadevan, V. S., Transcatheter pulmonary valve implantation: will it replace surgical pulmonary valve replacement? *Expert Rev Cardiovasc Ther* **2018,** *16* (3), 197-207.
5. Zhou, Y.; Xiong, T.; Bai, P.; Chu, C.; Dong, N., Clinical outcomes of transcatheter versus surgical pulmonary valve replacement: a meta-analysis. *J Thorac Dis* **2019,** *11* (12), 5343-5351.
6. Kwak, J. G.; Bang, J. H.; Cho, S.; Kim, E. R.; Shih, B. C.; Lee, C. H.; Kim, W. H., Long-term durability of bioprosthetic valves in pulmonary position: Pericardial versus porcine valves. *J Thorac Cardiovasc Surg* **2020,** *160* (2), 476-484.
7. Reimer, J.; Syedain, Z.; Haynie, B.; Lahti, M.; Berry, J.; Tranquillo, R., Implantation of a Tissue-Engineered Tubular Heart Valve in Growing Lambs. *Ann Biomed Eng* **2017,** *45* (2), 439-451.
8. Driesen, B. W.; Warmerdam, E. G.; Sieswerda, G. J.; Meijboom, F. J.; Molenschot, M. M. C.; Doevendans, P. A.; Krings, G. J.; van Dijk, A. P. J.; Voskuil, M., Percutaneous Pulmonary Valve Implantation: Current Status and Future Perspectives. *Curr Cardiol Rev* **2019,** *15* (4), 262-273.
9. Schievano, S.; Capelli, C.; Young, C.; Lurz, P.; Nordmeyer, J.; Owens, C.; Bonhoeffer, P.; Taylor, A. M., Four-dimensional computed tomography: a method of assessing right ventricular outflow tract and pulmonary artery deformations throughout the cardiac cycle. *Eur Radiol* **2011,** *21* (1), 36-45.
10. Buzzatti, N.; Maisano, F.; Latib, A.; Cioni, M.; Taramasso, M.; Mussardo, M.; Colombo, A.; Alfieri, O., Computed tomography-based evaluation of aortic annulus, prosthesis size and impact on early residual aortic regurgitation after transcatheter aortic valve implantation. *Eur J Cardiothorac Surg* **2013,** *43* (1), 43-50; discussion 50-1.
11. Détaint, D.; Lepage, L.; Himbert, D.; Brochet, E.; Messika-Zeitoun, D.; Iung, B.; Vahanian, A., Determinants of significant paravalvular regurgitation after transcatheter aortic valve: implantation impact of device and annulus discongruence. *JACC Cardiovasc Interv* **2009,** *2* (9), 821-7.
12. Hamdan, A.; Guetta, V.; Konen, E.; Goitein, O.; Segev, A.; Raanani, E.; Spiegelstein, D.; Hay, I.; Di Segni, E.; Eldar, M.; Schwammenthal, E., Deformation dynamics and mechanical properties of the aortic annulus by 4-dimensional computed tomography: insights into the functional anatomy of the aortic valve complex and implications for transcatheter aortic valve therapy. *J Am Coll Cardiol* **2012,** *59* (2), 119-27.
13. Ortuño, J. E.; Vegas-Sánchez-Ferrero, G.; Gómez-Valverde, J. J.; Chen, M. Y.; Santos, A.; McVeigh, E. R.; Ledesma-Carbayo, M. J., Automatic estimation of aortic and

mitral valve displacements in dynamic CTA with 4D graph-cuts. *Med Image Anal* **2020,** *65*, 101748.
14. Basra, S. S.; Gopal, A.; Hebeler, K. R.; Baumgarten, H.; Anderson, A.; Potluri, S. P.; Brinkman, W. T.; Szerlip, M.; Gopal, D.; Filardo, G.; DiMaio, J. M.; Brown, D. L.; Grayburn, P. A.; Mack, M. J.; Holper, E. M., Clinical Leaflet Thrombosis in Transcatheter and Surgical Bioprosthetic Aortic Valves by Four-Dimensional Computed Tomography. *Ann Thorac Surg* **2018,** *106* (6), 1716-1725.
15. Elattar, M. A.; Vink, L. W.; van Mourik, M. S.; Baan, J., Jr.; vanBavel, E. T.; Planken, R. N.; Marquering, H. A., Dynamics of the aortic annulus in 4D CT angiography for transcatheter aortic valve implantation patients. *PLoS One* **2017,** *12* (9), e0184133.
16. Madukauwa-David, I. D.; Midha, P. A.; Sharma, R.; McLain, K.; Mitra, R.; Crawford, K.; Yoon, S. H.; Makkar, R. R.; Yoganathan, A. P., Characterization of aortic root geometry in transcatheter aortic valve replacement patients. *Catheter Cardiovasc Interv* **2019,** *93* (1), 134-140.
17. Mauri, V.; Frohn, T.; Deuschl, F.; Mohemed, K.; Kuhr, K.; Reimann, A.; Körber, M. I.; Schofer, N.; Adam, M.; Friedrichs, K.; Kuhn, E. W.; Scholtz, S.; Rudolph, V.; Wahlers, T. C. W.; Baldus, S.; Mader, N.; Schäfer, U.; Rudolph, T. K., Impact of device landing zone calcification patterns on paravalvular regurgitation after transcatheter aortic valve replacement with different next-generation devices. *Open Heart* **2020,** *7* (1).
18. Sun, X.; Hao, Y.; Sebastian Kiekenap, J. F.; Emeis, J.; Steitz, M.; Breitenstein-Attach, A.; Berger, F.; Schmitt, B., Four-Dimensional Computed Tomography-Guided Valve Sizing for Transcatheter Pulmonary Valve Replacement. *J Vis Exp* **2022,** (179).
19. Hao, Y.; Sun, X.; Kiekenap, J. F. S.; Emeis, J.; Steitz, M.; Breitenstein-Attach, A.; Berger, F.; Schmitt, B., Transcatheter Pulmonary Valve Replacement from Autologous Pericardium with a Self-Expandable Nitinol Stent in an Adult Sheep Model. *J Vis Exp* **2022,** (184).
20. Chen, S. J.; Lin, M. T.; Liu, K. L.; Chang, C. I.; Chen, H. Y.; Wang, J. K.; Lee, W. J.; Tsang, Y. M.; Li, Y. W., Usefulness of 3D reconstructed computed tomography imaging for double outlet right ventricle. *J Formos Med Assoc* **2008,** *107* (5), 371-80.
21. Moore, C. C.; McVeigh, E. R.; Zerhouni, E. A., Quantitative tagged magnetic resonance imaging of the normal human left ventricle. *Top Magn Reson Imaging* **2000,** *11* (6), 359-71.
22. Finch, W.; Levi, D. S.; Salem, M.; Hageman, A.; Aboulhosn, J., Transcatheter melody valve placement in large diameter bioprostheses and conduits: What is the optimal "Landing zone"? *Catheter Cardiovasc Interv* **2015,** *86* (5), E217-23.
23. Schievano, S.; Coats, L.; Migliavacca, F.; Norman, W.; Frigiola, A.; Deanfield, J.; Bonhoeffer, P.; Taylor, A. M., Variations in right ventricular outflow tract morphology following repair of congenital heart disease: implications for percutaneous pulmonary valve implantation. *J Cardiovasc Magn Reson* **2007,** *9* (4), 687-95.
24. Zerhouni, E. A.; Parish, D. M.; Rogers, W. J.; Yang, A.; Shapiro, E. P., Human heart: tagging with MR imaging--a method for noninvasive assessment of myocardial motion. *Radiology* **1988,** *169* (1), 59-63.
25. Curran, L.; Agrawal, H.; Kallianos, K.; Kheiwa, A.; Lin, S.; Ordovas, K.; Mahadevan, V. S., Computed tomography guided sizing for transcatheter pulmonary valve replacement. *Int J Cardiol Heart Vasc* **2020,** *29*, 100523.
26. Pluchinotta, F. R.; Sturla, F.; Caimi, A.; Giugno, L.; Chessa, M.; Giamberti, A.; Votta, E.; Redaelli, A.; Carminati, M., 3-Dimensional personalized planning for transcatheter pulmonary valve implantation in a dysfunctional right ventricular outflow tract. *Int J Cardiol* **2020,** *309*, 33-39.

27. Chuang, M. A.; Akodad, M.; Chatfield, A. G.; Wood, D.; Sathananthan, J.; Leipsic, J. A.; Blanke, P.; Cheung, A.; Webb, J. G.; Ye, J., Stent Frame Fracture and Late Atrial Migration of a Mitral SAPIEN 3 Transcatheter Valve. *JACC Cardiovasc Interv* **2021,** *14* (14), 1610-1612.
28. Sun, X.; Hao, Y.; Steitz, M.; Breitenstein-Attach, A.; Kiekenap, J. F. S.; Emeis, J.; Khan, M. B.; Berger, F.; Schmitt, B., Straightened Segmentation in 4D Cardiac CT: A Practical Method for Multiparametric Characterization of the Landing Zone for Transcatheter Pulmonary Valve Replacement. *Applied Sciences* **2022,** *12* (24).
29. Schymik, G.; Heimeshoff, M.; Bramlage, P.; Wondraschek, R.; Süselbeck, T.; Gerhardus, J.; Luik, A.; Posival, H.; Schmitt, C.; Schröfel, H., Ruptures of the device landing zone in patients undergoing transcatheter aortic valve implantation: an analysis of TAVI Karlsruhe (TAVIK) patients. *Clin Res Cardiol* **2014,** *103* (11), 912-20.
30. Bruns, S.; Wolterink, J. M.; van den Boogert, T. P. W.; Runge, J. H.; Bouma, B. J.; Henriques, J. P.; Baan, J.; Viergever, M. A.; Planken, R. N.; Išgum, I., Deep learning-based whole-heart segmentation in 4D contrast-enhanced cardiac CT. *Comput Biol Med* **2022,** *142*, 105191.

Statutory Declaration

“I, [Yimeng,Hao], by personally signing this document in lieu of an oath, hereby affirm that I prepared the submitted dissertation on the topic [**The application of 4D cardiac CT segmentation for pre-operative and post-operative transcatheter pulmonary valve replacement; Die Anwendung der 4D-Segmentierung der Herz-CT für den prä- und postoperativen Transkatheter-Lungenklappenersatz**], independently and without the support of third parties, and that I used no other sources and aids than those stated.

All parts which are based on the publications or presentations of other authors, either in letter or in spirit, are specified as such in accordance with the citing guidelines. The sections on methodology (in particular regarding practical work, laboratory regulations, statistical processing) and results (in particular regarding figures, charts and tables) are exclusively my responsibility.

Furthermore, I declare that I have correctly marked all of the data, the analyses, and the conclusions generated from data obtained in collaboration with other persons, and that I have correctly marked my own contribution and the contributions of other persons (cf. declaration of contribution). I have correctly marked all texts or parts of texts that were generated in collaboration with other persons.

My contributions to any publications to this dissertation correspond to those stated in the below joint declaration made together with the supervisor. All publications created within the scope of the dissertation comply with the guidelines of the ICMJE (International Committee of Medical Journal Editors; www.icmje.org) on authorship. In addition, I declare that I shall comply with the regulations of Charité – Universitätsmedizin Berlin on ensuring good scientific practice.

I declare that I have not yet submitted this dissertation in identical or similar form to another Faculty.

The significance of this statutory declaration and the consequences of a false statutory declaration under criminal law (Sections 156, 161 of the German Criminal Code) are known to me.”

_____	_____
Date	Signature

Declaration of your own contribution to the publications

Yimeng Hao contributed the following to the below listed publications:

Publication 1: **Hao Y**, Sun X, Kiekenap JFS, Emeis J, Steitz M, Breitenstein-Attach A, Berger F, Schmitt B. Transcatheter Pulmonary Valve Replacement from Autologous Pericardium with a Self-Expandable Nitinol Stent in an Adult Sheep Model. J Vis Exp. 2022 Jun 8;(184).

Contribution: Participating in the animal experiment, including pre-operative preparation (medication, experimental instrument, and equipment), pre-medication administration, performing the anesthesia for the procedure (intravenous catheter placement, anesthesia induction, intubation, and gastric tube placement), and performing the experimental animal perioperative management (pre- and post-operative animal care, intraoperative hemodynamics, internal environment, and fluid management). Collection and organization of experimental data, including hemodynamic parameters and blood gas analysis results. Performing the literature searches. Participating in first draft writing and revision according to the reviewer's comments after the peer review.

Publication 2: Sun X*****, **Hao Y***, Sebastian Kiekenap JF, Emeis J, Steitz M, Breitenstein-Attach A, Berger F, Schmitt B. Four-Dimensional Computed Tomography-Guided Valve Sizing for Transcatheter Pulmonary Valve Replacement. J Vis Exp. 2022 Jan 20;(179).

*Share first authorship.

Contribution: Participating in the animal experiment, performing the anesthesia for the procedure. Performing the anatomical model reconstruction. Creating figure1, 2, and 6. Participating in first draft writing and revision according to the reviewer's comments after the peer review.

Publication 3: Sun X*****, **Hao Y***, Steitz M, Breitenstein-Attach A, Sebastian Kiekenap JF, Emeis J, Khan MB, Berger F, Schmitt B. Straightened Segmentation in 4D Cardiac CT: A Practical Method for Multiparametric Characterization of the Landing Zone for Transcatheter Pulmonary Valve Replacement. Appl. Sci. 2022, 12, 12912.

*Share first authorship.

Contribution: Contributed to the animal experiment, performing the anesthesia for the procedure. Performing the anatomical model reconstruction. Contributed to the conceptualization, methodology, formal analysis, data curation, the original draft writing

and editing according to the reviewer's comments after the peer review. All the figures and tables were created on the basis of my statistical evaluation.

_____

Signature, date and stamp of first supervising university professor / lecturer

_____

Signature of doctoral candidate

Excerpt from the Journal Summary List

Journal Data Filtered By: **Selected JCR Year: 2020** Selected Editions: SCIE,SSCI Selected Categories: **"MULTIDISCIPLINARY SCIENCES"** Selected Category Scheme: WoS

Gesamtanzahl: 73 Journale

Rank	Full Journal Title	Total Cites	Journal Impact Factor	Eigenfactor Score
1	NATURE	915,925	49.962	1.089400
2	SCIENCE	814,971	47.728	0.895760
3	National Science Review	5,889	17.275	0.011400
4	Nature Communications	453,215	14.919	1.238540
5	Science Advances	65,205	14.136	0.218640
6	Nature Human Behaviour	5,549	13.663	0.023120
7	Science Bulletin	8,832	11.780	0.016400
8	PROCEEDINGS OF THE NATIONAL ACADEMY OF SCIENCES OF THE UNITED STATES OF AMERICA	799,058	11.205	0.806620
9	Journal of Advanced Research	5,927	10.479	0.006800
10	GigaScience	5,876	6.524	0.018630
11	Scientific Data	10,617	6.444	0.034470
12	Frontiers in Bioengineering and Biotechnology	7,470	5.890	0.011340
13	ANNALS OF THE NEW YORK ACADEMY OF SCIENCES	52,619	5.691	0.021430
14	iScience	5,235	5.458	0.012300
15	Research Synthesis Methods	3,926	5.273	0.007520
16	NPJ Microgravity	594	4.415	0.001790
17	Scientific Reports	541,615	4.379	1.232500
18	PHILOSOPHICAL TRANSACTIONS OF THE ROYAL SOCIETY A-MATHEMATICAL PHYSICAL AND ENGINEERING SCIENCES	24,950	4.226	0.025400

Rank	Full Journal Title	Total Cites	Journal Impact Factor	Eigenfactor Score
19	Journal of the Royal Society Interface	16,834	4.118	0.022010
20	JOURNAL OF KING SAUD UNIVERSITY SCIENCE	3,276	4.011	0.002870
21	Advanced Theory and Simulations	1,201	4.004	0.002780
22	GLOBAL CHALLENGES	1,047	3.847	0.002860
23	FRACTALS-COMPLEX GEOMETRY PATTERNS AND SCALING IN NATURE AND SOCIETY	2,667	3.665	0.002570
24	SCIENCE AND ENGINEERING ETHICS	2,796	3.525	0.003700
25	PROCEEDINGS OF THE JAPAN ACADEMY SERIES B-PHYSICAL AND BIOLOGICAL SCIENCES	2,218	3.493	0.001940
26	PLoS One	857,723	3.240	1.081150
27	PeerJ	29,906	2.984	0.069540
28	Royal Society Open Science	11,155	2.963	0.030990
29	INTERNATIONAL JOURNAL OF BIFURCATION AND CHAOS	8,572	2.836	0.006590
30	COMPLEXITY	7,133	2.833	0.009620
31	SCIENCE PROGRESS	689	2.774	0.000380
32	JOURNAL OF THE ROYAL SOCIETY OF NEW ZEALAND	944	2.750	0.000680
33	Symmetry-Basel	9,999	2.713	0.011650
34	PROCEEDINGS OF THE ROYAL SOCIETY A-MATHEMATICAL PHYSICAL AND ENGINEERING SCIENCES	22,295	2.704	0.015330
35	Journal of Taibah University for Science	2,141	2.688	0.002210
36	MIT Technology Review	1,156	2.563	0.002680
37	Facets	488	2.535	0.001170

Selected JCR Year: 2020; Selected Categories: “MULTIDISCIPLINARY SCIENCES”

Rank	Full Journal Title	Total Cites	Journal Impact Factor	Eigenfactor Score
38	ARABIAN JOURNAL FOR SCIENCE AND ENGINEERING	8,349	2.334	0.008350
39	SOUTH AFRICAN JOURNAL OF SCIENCE	3,313	2.197	0.001680
40	SCIENTIFIC AMERICAN	7,590	2.142	0.003070
41	Frontiers in Life Science	520	2.000	0.000800
42	Science of Nature	954	1.954	0.002580
43	Journal of Radiation Research and Applied Sciences	1,611	1.770	0.001870
44	ANAIS DA ACADEMIA BRASILEIRA DE CIENCIAS	4,708	1.753	0.004490
45	JOURNAL OF THE INDIAN INSTITUTE OF SCIENCE	561	1.742	0.000510
46	RENDICONTI LINCEI-SCIENZE FISICHE E NATURALI	1,217	1.627	0.001380
47	PROCEEDINGS OF THE NATIONAL ACADEMY OF SCIENCES INDIA SECTION A-PHYSICAL SCIENCES	658	1.544	0.000850
48	Proceedings of the Romanian Academy Series A-Mathematics Physics Technical Sciences Information Science	485	1.523	0.000680
49	Jove-Journal of Visualized Experiments	20,722	1.355	0.031050
50	DISCRETE DYNAMICS IN NATURE AND SOCIETY	2,504	1.348	0.002530
51	ISSUES IN SCIENCE AND TECHNOLOGY	607	1.255	0.001080
52	ADVANCES IN COMPLEX SYSTEMS	677	1.226	0.000540
53	Iranian Journal of Science and Technology Transaction A-Science	1,237	1.194	0.001790
54	CURRENT SCIENCE	13,179	1.102	0.006070
55	Proceedings of the Estonian Academy of Sciences	638	1.045	0.000350
56	Sains Malaysiana	2,386	1.009	0.001890
57	INTERDISCIPLINARY SCIENCE REVIEWS	391	1.000	0.000250

Selected JCR Year: 2020; Selected Categories: "MULTIDISCIPLINARY SCIENCES"

Publication 1: Transcatheter Pulmonary Valve Replacement from Autologous Pericardium with a Self-Expandable Nitinol Stent in an Adult Sheep Model.

Hao Y, Sun X, Kiekenap JFS, Emeis J, Steitz M, Breitenstein-Attach A, Berger F, Schmitt B. Transcatheter Pulmonary Valve Replacement from Autologous Pericardium with a Self-Expandable Nitinol Stent in an Adult Sheep Model. J Vis Exp. 2022 Jun 8;(184). https://doi.org/10.3791/63661

Transcatheter Pulmonary Valve Replacement from Autologous Pericardium with a Self-Expandable Nitinol Stent in an Adult Sheep Model.

Hao Y, Sun X, Kiekenap JFS, Emeis J, Steitz M, Breitenstein-Attach A, Berger F, Schmitt B. Transcatheter Pulmonary Valve Replacement from Autologous Pericardium with a Self-Expandable Nitinol Stent in an Adult Sheep Model. J Vis Exp. 2022 Jun 8;(184). https://doi.org/10.3791/63661

Transcatheter Pulmonary Valve Replacement from Autologous Pericardium with a Self-Expandable Nitinol Stent in an Adult Sheep Model.

Hao Y, Sun X, Kiekenap JFS, Emeis J, Steitz M, Breitenstein-Attach A, Berger F, Schmitt B. Transcatheter Pulmonary Valve Replacement from Autologous Pericardium with a Self-Expandable Nitinol Stent in an Adult Sheep Model. J Vis Exp. 2022 Jun 8;(184). https://doi.org/10.3791/63661

Transcatheter Pulmonary Valve Replacement from Autologous Pericardium with a Self-Expandable Nitinol Stent in an Adult Sheep Model.

Hao Y, Sun X, Kiekenap JFS, Emeis J, Steitz M, Breitenstein-Attach A, Berger F, Schmitt B. Transcatheter Pulmonary Valve Replacement from Autologous Pericardium with a Self-Expandable Nitinol Stent in an Adult Sheep Model. J Vis Exp. 2022 Jun 8;(184). https://doi.org/10.3791/63661

Transcatheter Pulmonary Valve Replacement from Autologous Pericardium with a Self-Expandable Nitinol Stent in an Adult Sheep Model.

Hao Y, Sun X, Kiekenap JFS, Emeis J, Steitz M, Breitenstein-Attach A, Berger F, Schmitt B. Transcatheter Pulmonary Valve Replacement from Autologous Pericardium with a Self-Expandable Nitinol Stent in an Adult Sheep Model. J Vis Exp. 2022 Jun 8;(184). https://doi.org/10.3791/63661

Transcatheter Pulmonary Valve Replacement from Autologous Pericardium with a Self-Expandable Nitinol Stent in an Adult Sheep Model.

Hao Y, Sun X, Kiekenap JFS, Emeis J, Steitz M, Breitenstein-Attach A, Berger F, Schmitt B. Transcatheter Pulmonary Valve Replacement from Autologous Pericardium with a Self-Expandable Nitinol Stent in an Adult Sheep Model. J Vis Exp. 2022 Jun 8;(184). https://doi.org/10.3791/63661

Transcatheter Pulmonary Valve Replacement from Autologous Pericardium with a Self-Expandable Nitinol Stent in an Adult Sheep Model.

Hao Y, Sun X, Kiekenap JFS, Emeis J, Steitz M, Breitenstein-Attach A, Berger F, Schmitt B. Transcatheter Pulmonary Valve Replacement from Autologous Pericardium with a Self-Expandable Nitinol Stent in an Adult Sheep Model. J Vis Exp. 2022 Jun 8;(184). https://doi.org/10.3791/63661

Transcatheter Pulmonary Valve Replacement from Autologous Pericardium with a Self-Expandable Nitinol Stent in an Adult Sheep Model.

Hao Y, Sun X, Kiekenap JFS, Emeis J, Steitz M, Breitenstein-Attach A, Berger F, Schmitt B. Transcatheter Pulmonary Valve Replacement from Autologous Pericardium with a Self-Expandable Nitinol Stent in an Adult Sheep Model. J Vis Exp. 2022 Jun 8;(184). https://doi.org/10.3791/63661

Transcatheter Pulmonary Valve Replacement from Autologous Pericardium with a Self-Expandable Nitinol Stent in an Adult Sheep Model.

Hao Y, Sun X, Kiekenap JFS, Emeis J, Steitz M, Breitenstein-Attach A, Berger F, Schmitt B. Transcatheter Pulmonary Valve Replacement from Autologous Pericardium with a Self-Expandable Nitinol Stent in an Adult Sheep Model. J Vis Exp. 2022 Jun 8;(184). https://doi.org/10.3791/63661

Transcatheter Pulmonary Valve Replacement from Autologous Pericardium with a Self-Expandable Nitinol Stent in an Adult Sheep Model.

Hao Y, Sun X, Kiekenap JFS, Emeis J, Steitz M, Breitenstein-Attach A, Berger F, Schmitt B. Transcatheter Pulmonary Valve Replacement from Autologous Pericardium with a Self-Expandable Nitinol Stent in an Adult Sheep Model. J Vis Exp. 2022 Jun 8;(184). https://doi.org/10.3791/63661

Transcatheter Pulmonary Valve Replacement from Autologous Pericardium with a Self-Expandable Nitinol Stent in an Adult Sheep Model.

Hao Y, Sun X, Kiekenap JFS, Emeis J, Steitz M, Breitenstein-Attach A, Berger F, Schmitt B. Transcatheter Pulmonary Valve Replacement from Autologous Pericardium with a Self-Expandable Nitinol Stent in an Adult Sheep Model. J Vis Exp. 2022 Jun 8;(184). https://doi.org/10.3791/63661

Transcatheter Pulmonary Valve Replacement from Autologous Pericardium with a Self-Expandable Nitinol Stent in an Adult Sheep Model.

Hao Y, Sun X, Kiekenap JFS, Emeis J, Steitz M, Breitenstein-Attach A, Berger F, Schmitt B. Transcatheter Pulmonary Valve Replacement from Autologous Pericardium with a Self-Expandable Nitinol Stent in an Adult Sheep Model. J Vis Exp. 2022 Jun 8;(184). https://doi.org/10.3791/63661

Transcatheter Pulmonary Valve Replacement from Autologous Pericardium with a Self-Expandable Nitinol Stent in an Adult Sheep Model.

Hao Y, Sun X, Kiekenap JFS, Emeis J, Steitz M, Breitenstein-Attach A, Berger F, Schmitt B. Transcatheter Pulmonary Valve Replacement from Autologous Pericardium with a Self-Expandable Nitinol Stent in an Adult Sheep Model. J Vis Exp. 2022 Jun 8;(184). https://doi.org/10.3791/63661

Transcatheter Pulmonary Valve Replacement from Autologous Pericardium with a Self-Expandable Nitinol Stent in an Adult Sheep Model.

Hao Y, Sun X, Kiekenap JFS, Emeis J, Steitz M, Breitenstein-Attach A, Berger F, Schmitt B. Transcatheter Pulmonary Valve Replacement from Autologous Pericardium with a Self-Expandable Nitinol Stent in an Adult Sheep Model. J Vis Exp. 2022 Jun 8;(184). https://doi.org/10.3791/63661

Transcatheter Pulmonary Valve Replacement from Autologous Pericardium with a Self-Expandable Nitinol Stent in an Adult Sheep Model.

Hao Y, Sun X, Kiekenap JFS, Emeis J, Steitz M, Breitenstein-Attach A, Berger F, Schmitt B. Transcatheter Pulmonary Valve Replacement from Autologous Pericardium with a Self-Expandable Nitinol Stent in an Adult Sheep Model. J Vis Exp. 2022 Jun 8;(184). https://doi.org/10.3791/63661

Transcatheter Pulmonary Valve Replacement from Autologous Pericardium with a Self-Expandable Nitinol Stent in an Adult Sheep Model.

Hao Y, Sun X, Kiekenap JFS, Emeis J, Steitz M, Breitenstein-Attach A, Berger F, Schmitt B. Transcatheter Pulmonary Valve Replacement from Autologous Pericardium with a Self-Expandable Nitinol Stent in an Adult Sheep Model. J Vis Exp. 2022 Jun 8;(184). https://doi.org/10.3791/63661

Transcatheter Pulmonary Valve Replacement from Autologous Pericardium with a Self-Expandable Nitinol Stent in an Adult Sheep Model.

Hao Y, Sun X, Kiekenap JFS, Emeis J, Steitz M, Breitenstein-Attach A, Berger F, Schmitt B. Transcatheter Pulmonary Valve Replacement from Autologous Pericardium with a Self-Expandable Nitinol Stent in an Adult Sheep Model. J Vis Exp. 2022 Jun 8;(184). https://doi.org/10.3791/63661

Transcatheter Pulmonary Valve Replacement from Autologous Pericardium with a Self-Expandable Nitinol Stent in an Adult Sheep Model.

Hao Y, Sun X, Kiekenap JFS, Emeis J, Steitz M, Breitenstein-Attach A, Berger F, Schmitt B. Transcatheter Pulmonary Valve Replacement from Autologous Pericardium with a Self-Expandable Nitinol Stent in an Adult Sheep Model. J Vis Exp. 2022 Jun 8;(184). https://doi.org/10.3791/63661

Transcatheter Pulmonary Valve Replacement from Autologous Pericardium with a Self-Expandable Nitinol Stent in an Adult Sheep Model.

Hao Y, Sun X, Kiekenap JFS, Emeis J, Steitz M, Breitenstein-Attach A, Berger F, Schmitt B. Transcatheter Pulmonary Valve Replacement from Autologous Pericardium with a Self-Expandable Nitinol Stent in an Adult Sheep Model. J Vis Exp. 2022 Jun 8;(184). https://doi.org/10.3791/63661

Transcatheter Pulmonary Valve Replacement from Autologous Pericardium with a Self-Expandable Nitinol Stent in an Adult Sheep Model.

Hao Y, Sun X, Kiekenap JFS, Emeis J, Steitz M, Breitenstein-Attach A, Berger F, Schmitt B. Transcatheter Pulmonary Valve Replacement from Autologous Pericardium with a Self-Expandable Nitinol Stent in an Adult Sheep Model. J Vis Exp. 2022 Jun 8;(184). https://doi.org/10.3791/63661

Transcatheter Pulmonary Valve Replacement from Autologous Pericardium with a Self-Expandable Nitinol Stent in an Adult Sheep Model.

Hao Y, Sun X, Kiekenap JFS, Emeis J, Steitz M, Breitenstein-Attach A, Berger F, Schmitt B. Transcatheter Pulmonary Valve Replacement from Autologous Pericardium with a Self-Expandable Nitinol Stent in an Adult Sheep Model. J Vis Exp. 2022 Jun 8;(184). https://doi.org/10.3791/63661

Transcatheter Pulmonary Valve Replacement from Autologous Pericardium with a Self-Expandable Nitinol Stent in an Adult Sheep Model.

Hao Y, Sun X, Kiekenap JFS, Emeis J, Steitz M, Breitenstein-Attach A, Berger F, Schmitt B. Transcatheter Pulmonary Valve Replacement from Autologous Pericardium with a Self-Expandable Nitinol Stent in an Adult Sheep Model. J Vis Exp. 2022 Jun 8;(184). https://doi.org/10.3791/63661

Transcatheter Pulmonary Valve Replacement from Autologous Pericardium with a Self-Expandable Nitinol Stent in an Adult Sheep Model.

Hao Y, Sun X, Kiekenap JFS, Emeis J, Steitz M, Breitenstein-Attach A, Berger F, Schmitt B. Transcatheter Pulmonary Valve Replacement from Autologous Pericardium with a Self-Expandable Nitinol Stent in an Adult Sheep Model. J Vis Exp. 2022 Jun 8;(184). https://doi.org/10.3791/63661

Transcatheter Pulmonary Valve Replacement from Autologous Pericardium with a Self-Expandable Nitinol Stent in an Adult Sheep Model.

Hao Y, Sun X, Kiekenap JFS, Emeis J, Steitz M, Breitenstein-Attach A, Berger F, Schmitt B. Transcatheter Pulmonary Valve Replacement from Autologous Pericardium with a Self-Expandable Nitinol Stent in an Adult Sheep Model. J Vis Exp. 2022 Jun 8;(184). https://doi.org/10.3791/63661

Journal Data Filtered By: **Selected JCR Year: 2020** Selected Editions: SCIE,SSCI Selected Categories: **"MULTIDISCIPLINARY SCIENCES"** Selected Category Scheme: WoS

Gesamtanzahl: 73 Journale

Rank	Full Journal Title	Total Cites	Journal Impact Factor	Eigenfactor Score
1	NATURE	915,925	49.962	1.089400
2	SCIENCE	814,971	47.728	0.895760
3	National Science Review	5,889	17.275	0.011400
4	Nature Communications	453,215	14.919	1.238540
5	Science Advances	65,205	14.136	0.218640
6	Nature Human Behaviour	5,549	13.663	0.023120
7	Science Bulletin	8,832	11.780	0.016400
8	PROCEEDINGS OF THE NATIONAL ACADEMY OF SCIENCES OF THE UNITED STATES OF AMERICA	799,058	11.205	0.806620
9	Journal of Advanced Research	5,927	10.479	0.006800
10	GigaScience	5,876	6.524	0.018630
11	Scientific Data	10,617	6.444	0.034470
12	Frontiers in Bioengineering and Biotechnology	7,470	5.890	0.011340
13	ANNALS OF THE NEW YORK ACADEMY OF SCIENCES	52,619	5.691	0.021430
14	iScience	5,235	5.458	0.012300
15	Research Synthesis Methods	3,926	5.273	0.007520
16	NPJ Microgravity	594	4.415	0.001790
17	Scientific Reports	541,615	4.379	1.232500
18	PHILOSOPHICAL TRANSACTIONS OF THE ROYAL SOCIETY A-MATHEMATICAL PHYSICAL AND ENGINEERING SCIENCES	24,950	4.226	0.025400

Rank	Full Journal Title	Total Cites	Journal Impact Factor	Eigenfactor Score
19	Journal of the Royal Society Interface	16,834	4.118	0.022010
20	JOURNAL OF KING SAUD UNIVERSITY SCIENCE	3,276	4.011	0.002870
21	Advanced Theory and Simulations	1,201	4.004	0.002780
22	GLOBAL CHALLENGES	1,047	3.847	0.002860
23	FRACTALS-COMPLEX GEOMETRY PATTERNS AND SCALING IN NATURE AND SOCIETY	2,667	3.665	0.002570
24	SCIENCE AND ENGINEERING ETHICS	2,796	3.525	0.003700
25	PROCEEDINGS OF THE JAPAN ACADEMY SERIES B-PHYSICAL AND BIOLOGICAL SCIENCES	2,218	3.493	0.001940
26	PLoS One	857,723	3.240	1.081150
27	PeerJ	29,906	2.984	0.069540
28	Royal Society Open Science	11,155	2.963	0.030990
29	INTERNATIONAL JOURNAL OF BIFURCATION AND CHAOS	8,572	2.836	0.006590
30	COMPLEXITY	7,133	2.833	0.009620
31	SCIENCE PROGRESS	689	2.774	0.000380
32	JOURNAL OF THE ROYAL SOCIETY OF NEW ZEALAND	944	2.750	0.000680
33	Symmetry-Basel	9,999	2.713	0.011650
34	PROCEEDINGS OF THE ROYAL SOCIETY A-MATHEMATICAL PHYSICAL AND ENGINEERING SCIENCES	22,295	2.704	0.015330
35	Journal of Taibah University for Science	2,141	2.688	0.002210
36	MIT Technology Review	1,156	2.563	0.002680
37	Facets	488	2.535	0.001170

Selected JCR Year: 2020; Selected Categories: “MULTIDISCIPLINARY SCIENCES”

Rank	Full Journal Title	Total Cites	Journal Impact Factor	Eigenfactor Score
38	ARABIAN JOURNAL FOR SCIENCE AND ENGINEERING	8,349	2.334	0.008350
39	SOUTH AFRICAN JOURNAL OF SCIENCE	3,313	2.197	0.001680
40	SCIENTIFIC AMERICAN	7,590	2.142	0.003070
41	Frontiers in Life Science	520	2.000	0.000800
42	Science of Nature	954	1.954	0.002580
43	Journal of Radiation Research and Applied Sciences	1,611	1.770	0.001870
44	ANAIS DA ACADEMIA BRASILEIRA DE CIENCIAS	4,708	1.753	0.004490
45	JOURNAL OF THE INDIAN INSTITUTE OF SCIENCE	561	1.742	0.000510
46	RENDICONTI LINCEI-SCIENZE FISICHE E NATURALI	1,217	1.627	0.001380
47	PROCEEDINGS OF THE NATIONAL ACADEMY OF SCIENCES INDIA SECTION A-PHYSICAL SCIENCES	658	1.544	0.000850
48	Proceedings of the Romanian Academy Series A-Mathematics Physics Technical Sciences Information Science	485	1.523	0.000680
49	Jove-Journal of Visualized Experiments	20,722	1.355	0.031050
50	DISCRETE DYNAMICS IN NATURE AND SOCIETY	2,504	1.348	0.002530
51	ISSUES IN SCIENCE AND TECHNOLOGY	607	1.255	0.001080
52	ADVANCES IN COMPLEX SYSTEMS	677	1.226	0.000540
53	Iranian Journal of Science and Technology Transaction A-Science	1,237	1.194	0.001790
54	CURRENT SCIENCE	13,179	1.102	0.006070
55	Proceedings of the Estonian Academy of Sciences	638	1.045	0.000350
56	Sains Malaysiana	2,386	1.009	0.001890
57	INTERDISCIPLINARY SCIENCE REVIEWS	391	1.000	0.000250

Selected JCR Year: 2020; Selected Categories: "MULTIDISCIPLINARY SCIENCES"

Publication 2: Four-Dimensional Computed Tomography-Guided Valve Sizing for Transcatheter Pulmonary Valve Replacement.

Sun X*****, **Hao Y***, Sebastian Kiekenap JF, Emeis J, Steitz M, Breitenstein-Attach A, Berger F, Schmitt B. Four-Dimensional Computed Tomography-Guided Valve Sizing for Transcatheter Pulmonary Valve Replacement. J Vis Exp. 2022 Jan 20;(179).

https://doi.org/10.3791/63367

*Share first authorship.

Four-Dimensional Computed Tomography-Guided Valve Sizing for Transcatheter Pulmonary Valve Replacement.

Sun X*****, **Hao Y***, Sebastian Kiekenap JF, Emeis J, Steitz M, Breitenstein-Attach A, Berger F, Schmitt B. Four-Dimensional Computed Tomography-Guided Valve Sizing for Transcatheter Pulmonary Valve Replacement. J Vis Exp. 2022 Jan 20;(179).

https://doi.org/10.3791/63367

Four-Dimensional Computed Tomography-Guided Valve Sizing for Transcatheter Pulmonary Valve Replacement.

Sun X*****, **Hao Y***, Sebastian Kiekenap JF, Emeis J, Steitz M, Breitenstein-Attach A, Berger F, Schmitt B. Four-Dimensional Computed Tomography-Guided Valve Sizing for Transcatheter Pulmonary Valve Replacement. J Vis Exp. 2022 Jan 20;(179). https://doi.org/10.3791/63367

Four-Dimensional Computed Tomography-Guided Valve Sizing for Transcatheter Pulmonary Valve Replacement.

Sun X*****, **Hao Y***, Sebastian Kiekenap JF, Emeis J, Steitz M, Breitenstein-Attach A, Berger F, Schmitt B. Four-Dimensional Computed Tomography-Guided Valve Sizing for Transcatheter Pulmonary Valve Replacement. J Vis Exp. 2022 Jan 20;(179).

https://doi.org/10.3791/63367

Four-Dimensional Computed Tomography-Guided Valve Sizing for Transcatheter Pulmonary Valve Replacement.

Sun X*****, **Hao Y***, Sebastian Kiekenap JF, Emeis J, Steitz M, Breitenstein-Attach A, Berger F, Schmitt B. Four-Dimensional Computed Tomography-Guided Valve Sizing for Transcatheter Pulmonary Valve Replacement. J Vis Exp. 2022 Jan 20;(179).

https://doi.org/10.3791/63367

Four-Dimensional Computed Tomography-Guided Valve Sizing for Transcatheter Pulmonary Valve Replacement.

Sun X*, **Hao Y***, Sebastian Kiekenap JF, Emeis J, Steitz M, Breitenstein-Attach A, Berger F, Schmitt B. Four-Dimensional Computed Tomography-Guided Valve Sizing for Transcatheter Pulmonary Valve Replacement. J Vis Exp. 2022 Jan 20;(179).

https://doi.org/10.3791/63367

Four-Dimensional Computed Tomography-Guided Valve Sizing for Transcatheter Pulmonary Valve Replacement.

Sun X*****, **Hao Y***, Sebastian Kiekenap JF, Emeis J, Steitz M, Breitenstein-Attach A, Berger F, Schmitt B. Four-Dimensional Computed Tomography-Guided Valve Sizing for Transcatheter Pulmonary Valve Replacement. J Vis Exp. 2022 Jan 20;(179).

https://doi.org/10.3791/63367

Four-Dimensional Computed Tomography-Guided Valve Sizing for Transcatheter Pulmonary Valve Replacement.

Sun X*****, **Hao Y***, Sebastian Kiekenap JF, Emeis J, Steitz M, Breitenstein-Attach A, Berger F, Schmitt B. Four-Dimensional Computed Tomography-Guided Valve Sizing for Transcatheter Pulmonary Valve Replacement. J Vis Exp. 2022 Jan 20;(179).

https://doi.org/10.3791/63367

Four-Dimensional Computed Tomography-Guided Valve Sizing for Transcatheter Pulmonary Valve Replacement.

Sun X*, **Hao Y***, Sebastian Kiekenap JF, Emeis J, Steitz M, Breitenstein-Attach A, Berger F, Schmitt B. Four-Dimensional Computed Tomography-Guided Valve Sizing for Transcatheter Pulmonary Valve Replacement. J Vis Exp. 2022 Jan 20;(179).

https://doi.org/10.3791/63367

Four-Dimensional Computed Tomography-Guided Valve Sizing for Transcatheter Pulmonary Valve Replacement.

Sun X*****, **Hao Y***, Sebastian Kiekenap JF, Emeis J, Steitz M, Breitenstein-Attach A, Berger F, Schmitt B. Four-Dimensional Computed Tomography-Guided Valve Sizing for Transcatheter Pulmonary Valve Replacement. J Vis Exp. 2022 Jan 20;(179).

https://doi.org/10.3791/63367

Four-Dimensional Computed Tomography-Guided Valve Sizing for Transcatheter Pulmonary Valve Replacement.

Sun X*****, **Hao Y***, Sebastian Kiekenap JF, Emeis J, Steitz M, Breitenstein-Attach A, Berger F, Schmitt B. Four-Dimensional Computed Tomography-Guided Valve Sizing for Transcatheter Pulmonary Valve Replacement. J Vis Exp. 2022 Jan 20;(179).

https://doi.org/10.3791/63367

Four-Dimensional Computed Tomography-Guided Valve Sizing for Transcatheter Pulmonary Valve Replacement.

Sun X*, **Hao Y***, Sebastian Kiekenap JF, Emeis J, Steitz M, Breitenstein-Attach A, Berger F, Schmitt B. Four-Dimensional Computed Tomography-Guided Valve Sizing for Transcatheter Pulmonary Valve Replacement. J Vis Exp. 2022 Jan 20;(179).

https://doi.org/10.3791/63367

Four-Dimensional Computed Tomography-Guided Valve Sizing for Transcatheter Pulmonary Valve Replacement.

Sun X*****, **Hao Y***, Sebastian Kiekenap JF, Emeis J, Steitz M, Breitenstein-Attach A, Berger F, Schmitt B. Four-Dimensional Computed Tomography-Guided Valve Sizing for Transcatheter Pulmonary Valve Replacement. J Vis Exp. 2022 Jan 20;(179). https://doi.org/10.3791/63367

Four-Dimensional Computed Tomography-Guided Valve Sizing for Transcatheter Pulmonary Valve Replacement.

Sun X*****, **Hao Y***, Sebastian Kiekenap JF, Emeis J, Steitz M, Breitenstein-Attach A, Berger F, Schmitt B. Four-Dimensional Computed Tomography-Guided Valve Sizing for Transcatheter Pulmonary Valve Replacement. J Vis Exp. 2022 Jan 20;(179).

https://doi.org/10.3791/63367

Four-Dimensional Computed Tomography-Guided Valve Sizing for Transcatheter Pulmonary Valve Replacement.

Sun X*, **Hao Y***, Sebastian Kiekenap JF, Emeis J, Steitz M, Breitenstein-Attach A, Berger F, Schmitt B. Four-Dimensional Computed Tomography-Guided Valve Sizing for Transcatheter Pulmonary Valve Replacement. J Vis Exp. 2022 Jan 20;(179).

https://doi.org/10.3791/63367

Four-Dimensional Computed Tomography-Guided Valve Sizing for Transcatheter Pulmonary Valve Replacement.

Sun X*****, **Hao Y***, Sebastian Kiekenap JF, Emeis J, Steitz M, Breitenstein-Attach A, Berger F, Schmitt B. Four-Dimensional Computed Tomography-Guided Valve Sizing for Transcatheter Pulmonary Valve Replacement. J Vis Exp. 2022 Jan 20;(179). https://doi.org/10.3791/63367

Four-Dimensional Computed Tomography-Guided Valve Sizing for Transcatheter Pulmonary Valve Replacement.

Sun X*, **Hao Y***, Sebastian Kiekenap JF, Emeis J, Steitz M, Breitenstein-Attach A, Berger F, Schmitt B. Four-Dimensional Computed Tomography-Guided Valve Sizing for Transcatheter Pulmonary Valve Replacement. J Vis Exp. 2022 Jan 20;(179).

https://doi.org/10.3791/63367

Four-Dimensional Computed Tomography-Guided Valve Sizing for Transcatheter Pulmonary Valve Replacement.

Sun X*****, **Hao Y***, Sebastian Kiekenap JF, Emeis J, Steitz M, Breitenstein-Attach A, Berger F, Schmitt B. Four-Dimensional Computed Tomography-Guided Valve Sizing for Transcatheter Pulmonary Valve Replacement. J Vis Exp. 2022 Jan 20;(179).

https://doi.org/10.3791/63367

Four-Dimensional Computed Tomography-Guided Valve Sizing for Transcatheter Pulmonary Valve Replacement.

Sun X*, **Hao Y***, Sebastian Kiekenap JF, Emeis J, Steitz M, Breitenstein-Attach A, Berger F, Schmitt B. Four-Dimensional Computed Tomography-Guided Valve Sizing for Transcatheter Pulmonary Valve Replacement. J Vis Exp. 2022 Jan 20;(179).

https://doi.org/10.3791/63367

Journal Data Filtered By: **Selected JCR Year: 2021** Selected Editions: SCIE,SSCI
Selected Categories: **"MATERIALS SCIENCE, MULTIDISCIPLINARY"**
Selected Category Scheme: WoS
Gesamtanzahl: 346 Journale

Rank	Full Journal Title	Total Cites	Journal Impact Factor	Eigenfaktor
1	Nature Reviews Materials	27,820	76.679	0.06731
2	Nature Energy	37,355	67.439	0.08551
3	PROGRESS IN MATERIALS SCIENCE	25,960	48.165	0.01874
4	NATURE MATERIALS	119,078	47.656	0.12118
5	Joule	26,944	46.048	0.05961
6	Nature Nanotechnology	79,609	40.523	0.08705
7	MATERIALS SCIENCE & ENGINEERING R-REPORTS	9,517	33.667	0.00434
8	ADVANCED MATERIALS	361,407	32.086	0.40981
9	Advanced Energy Materials	116,667	29.698	0.16876
10	Materials Today	24,067	26.943	0.02238
11	InfoMat	3,447	24.798	0.00519
12	ACS Energy Letters	42,884	23.991	0.08474
13	Nano-Micro Letters	12,169	23.655	0.01283
14	Carbon Energy	1,341	21.556	0.00176
15	Energy Storage Materials	29,703	20.831	0.04216
16	Matter	6,917	19.967	0.01322
17	ADVANCED FUNCTIONAL MATERIALS	194,635	19.924	0.23063
18	Nano Energy	98,948	19.069	0.12429
19	Nano Today	13,207	18.962	0.01039
20	ACS Nano	224,439	18.027	0.22943
21	Advanced Science	42,938	17.521	0.06822

Rank	Full Journal Title	Total Cites	Journal Impact Factor	Eigenfaktor
22	INTERNATIONAL MATERIALS REVIEWS	7,790	15.750	0.00408
23	Materials Horizons	14,937	15.717	0.02209
24	Small Methods	10,967	15.367	0.01809
25	Small	97,357	15.153	0.10788
26	Journal of Materials Chemistry A	228,406	14.511	0.24055
27	Annual Review of Materials Research	9,768	13.972	0.00452
28	Energy & Environmental Materials	2,009	13.443	0.00259
29	Materials Today Nano	1,293	13.364	0.00191
30	Advanced Fiber Materials	756	12.958	0.00078
31	CURRENT OPINION IN SOLID STATE & MATERIALS SCIENCE	5,120	12.857	0.00347
32	NANO LETTERS	183,125	12.262	0.16870
33	npj Computational Materials	7,303	12.256	0.01647
34	EcoMat	766	12.213	0.00094
35	npj Flexible Electronics	1,331	12.019	0.00234
36	CEMENT AND CONCRETE RESEARCH	63,406	11.958	0.02190
37	Nanoscale Horizons	5,220	11.684	0.00842
38	Additive Manufacturing	22,892	11.632	0.02998
39	Small Structures	1,317	11.343	0.00078
40	CARBON	108,195	11.307	0.06982
41	CRITICAL REVIEWS IN SOLID STATE AND MATERIALS SCIENCES	2,380	11.178	0.00140
42	ACS Materials Letters	3,583	11.170	0.00606
43	Materials Today Physics	3,387	11.021	0.00428

Selected JCR Year: 2021; Selected Categories: “MATERIALS SCIENCE, MULTIDISCIPLINARY”

Rank	Full Journal Title	Total Cites	Journal Impact Factor	Eigenfaktor
44	Virtual and Physical Prototyping	2,725	10.962	0.00258
45	NPG Asia Materials	7,857	10.761	0.00958
46	Sustainable Materials and Technologies	2,912	10.681	0.00294
47	npj 2D Materials and Applications	2,184	10.516	0.00465
48	CHEMISTRY OF MATERIALS	130,194	10.508	0.11085
49	ACS Applied Materials & Interfaces	345,640	10.383	0.38051
50	JOURNAL OF MATERIALS SCIENCE & TECHNOLOGY	23,497	10.319	0.01911
51	Nano Research	29,620	10.269	0.03242
52	Advanced Optical Materials	27,344	10.050	0.04318
53	Nano Convergence	1,826	10.038	0.00222
54	International Journal of Extreme Manufacturing	648	10.036	0.00095
55	Materials Today Advances	1,057	9.918	0.00158
56	JOURNAL OF POWER SOURCES	157,002	9.794	0.09117
57	Advances in Nano Research	1,341	9.539	0.00097
58	MATERIALS & DESIGN	83,671	9.417	0.06232
59	Materials Today Energy	5,928	9.257	0.00694
60	ACTA MATERIALIA	112,177	9.209	0.07517
60	Solar RRL	9,310	9.173	0.01408
62	Advanced Materials Technologies	11,322	8.856	0.01849
63	Materials Chemistry Frontiers	10,417	8.683	0.01327
64	Applied Materials Today	8,849	8.663	0.01172
65	Science China-Materials	7,063	8.640	0.00907
66	Journal of Materiomics	3,329	8.589	0.00361

Selected JCR Year: 2021; Selected Categories: "MATERIALS SCIENCE, MULTIDISCIPLINARY"

Rank	Full Journal Title	Total Cites	Journal Impact Factor	Eigenfaktor
67	Materials Research Letters	4,363	8.516	0.00625
68	INTERNATIONAL JOURNAL OF PLASTICITY	17,762	8.500	0.01217
69	PROGRESS IN PHOTOVOLTAICS	9,014	8.490	0.00809
70	Nanoscale	141,429	8.307	0.14237
71	Journal of Materials Chemistry C	76,626	8.067	0.08707
72	Journal of Nanostructure in Chemistry	2,305	8.000	0.00158
73	Nanophotonics	8,535	7.923	0.01545
74	Cell Reports Physical Science	2,080	7.832	0.00335
75	SCIENCE AND TECHNOLOGY OF ADVANCED MATERIALS	7,338	7.821	0.00479
76	CORROSION SCIENCE	57,747	7.720	0.02441
77	CONSTRUCTION AND BUILDING MATERIALS	178,658	7.693	0.11196
78	Current Opinion in Electrochemistry	4,976	7.664	0.00765
79	Advanced Electronic Materials	12,682	7.633	0.02145
80	Materials Today Chemistry	3,355	7.613	0.00359
81	Journal of Physics-Energy	988	7.528	0.00154
82	Journal of Science-Advanced Materials and Devices	2,386	7.382	0.00256
83	SOLAR ENERGY MATERIALS AND SOLAR CELLS	38,448	7.305	0.02743
84	Materials Today Sustainability	409	7.244	0.00045
85	ACS Photonics	20,030	7.077	0.03960
86	ACS Applied Energy Materials	24,312	6.959	0.03678
87	npj Materials Degradation	1,229	6.889	0.00202
88	Journal of Physical Chemistry Letters	69,712	6.888	0.09047

Selected JCR Year: 2021; Selected Categories: “MATERIALS SCIENCE, MULTIDISCIPLINARY”

Rank	Full Journal Title	Total Cites	Journal Impact Factor	Eigenfaktor
89	2D Materials	10,005	6.861	0.01888
90	npj Quantum Materials	2,444	6.856	0.00790
91	Sustainable Energy & Fuels	10,267	6.813	0.01480
92	Nanotechnology Reviews	2,474	6.739	0.00220
93	Advanced Sustainable Systems	2,397	6.737	0.00358
94	APL Materials	9,229	6.635	0.01177
95	Advanced Materials Interfaces	18,339	6.389	0.02601
96	JOURNAL OF ALLOYS AND COMPOUNDS	186,355	6.371	0.13854
97	RARE METALS	6,165	6.318	0.00492
98	SCRIPTA MATERIALIA	47,388	6.302	0.03087
99	Journal of Materials Research and Technology-JMR&T	17,490	6.267	0.01618
100	JOURNAL OF MATERIALS PROCESSING TECHNOLOGY	45,159	6.162	0.02048
101	ACS Applied Nano Materials	19,177	6.140	0.02599
102	MATERIALS SCIENCE AND ENGINEERING A-STRUCTURAL MATERIALS PROPERTIES MICROSTRUCTURE AND PROCESSING	115,888	6.044	0.05728
103	Batteries & Supercaps	1,948	6.043	0.00300
104	Batteries-Basel	1,490	5.938	0.00211
105	APPLIED CLAY SCIENCE	26,604	5.907	0.01511
106	MICROPOROUS AND MESOPOROUS MATERIALS	36,750	5.876	0.01975
107	Journal of Physics-Materials	1,034	5.847	0.00227
108	FlatChem	945	5.829	0.00124
109	Nanomaterials	40,452	5.719	0.04213

Selected JCR Year: 2021; Selected Categories: "MATERIALS SCIENCE, MULTIDISCIPLINARY"

Rank	Full Journal Title	Total Cites	Journal Impact Factor	Eigenfaktor
110	MATERIALS RESEARCH BULLETIN	27,999	5.600	0.01235
111	Nanoscale Advances	6,647	5.598	0.00872
112	IUCrJ	3,165	5.588	0.00915
113	JOURNAL OF THE MECHANICS AND PHYSICS OF SOLIDS	27,635	5.582	0.01824
114	INTERNATIONAL JOURNAL OF FATIGUE	23,564	5.489	0.01638
115	Nanoscale Research Letters	22,557	5.418	0.01429
116	3D Printing and Additive Manufacturing	1,607	5.355	0.00135
117	Journal of Sustainable Cement-Based Materials	938	5.328	0.00070
118	REVIEWS ON ADVANCED MATERIALS SCIENCE	2,179	5.028	0.00107
119	Case Studies in Construction Materials	2,703	4.934	0.00263
120	Molecular Systems Design & Engineering	1,825	4.920	0.00353
121	MRS BULLETIN	9,321	4.882	0.00616
122	ACS Applied Polymer Materials	5,602	4.855	0.00693
123	INTERNATIONAL JOURNAL OF REFRACTORY METALS & HARD MATERIALS	10,911	4.804	0.00678
124	MATERIALS AND MANUFACTURING PROCESSES	8,918	4.783	0.00484
125	MATERIALS CHEMISTRY AND PHYSICS	44,833	4.778	0.02524
126	Extreme Mechanics Letters	4,363	4.728	0.00780
127	WEAR	37,494	4.695	0.01278
128	JOURNAL OF MATERIALS SCIENCE	69,454	4.682	0.03450
129	MATERIALS SCIENCE IN SEMICONDUCTOR PROCESSING	14,529	4.644	0.01039
130	GEOSYNTHETICS INTERNATIONAL	2,776	4.565	0.00189
131	Results in Physics	18,113	4.565	0.01960

Selected JCR Year: 2021; Selected Categories: “MATERIALS SCIENCE, MULTIDISCIPLINARY”

Rank	Full Journal Title	Total Cites	Journal Impact Factor	Eigenfaktor
132	Membranes	6,109	4.562	0.00479
133	MATERIALS CHARACTERIZATION	21,101	4.537	0.01746
134	ACS Applied Electronic Materials	4,185	4.494	0.00607
135	JOURNAL OF NON-CRYSTALLINE SOLIDS	34,388	4.458	0.01222
136	MACROMOLECULAR MATERIALS AND ENGINEERING	8,087	4.402	0.00525
137	IEEE Journal of Photovoltaics	7,755	4.401	0.00854
138	LANGMUIR	129,693	4.331	0.05406
139	MATERIALS AND STRUCTURES	17,191	4.285	0.00870
140	Progress in Natural Science-Materials International	6,692	4.269	0.00385
141	Journal of Information Display	553	4.237	0.00069
142	INTERNATIONAL JOURNAL FOR NUMERICAL AND ANALYTICAL METHODS IN GEOMECHANICS	8,942	4.229	0.00538
143	Journal of Physical Chemistry C	176,274	4.177	0.13014
144	MECHANICS OF MATERIALS	11,303	4.137	0.00702
145	Smart Materials and Structures	25,785	4.131	0.01763
146	ADVANCED ENGINEERING MATERIALS	16,228	4.122	0.01247
147	SCIENCE AND TECHNOLOGY OF WELDING AND JOINING	4,886	4.114	0.00221
148	VACUUM	17,655	4.110	0.01260
149	MICROSCOPY AND MICROANALYSIS	6,075	4.099	0.00634
150	INTERMETALLICS	15,562	4.075	0.00777
151	Nano Futures	372	4.070	0.00071
152	Soft Matter	46,522	4.046	0.03948
153	RAPID PROTOTYPING JOURNAL	8,079	4.043	0.00446

Selected JCR Year: 2021; Selected Categories: "MATERIALS SCIENCE, MULTIDISCIPLINARY"

Rank	Full Journal Title	Total Cites	Journal Impact Factor	Eigenfaktor
154	Archives of Civil and Mechanical Engineering	4,039	4.042	0.00345
155	CRYSTAL GROWTH & DESIGN	36,459	4.010	0.02481
156	International Journal of Smart and Nano Materials	638	4.000	0.00048
157	SYNTHETIC METALS	15,080	4.000	0.00556
158	INTERNATIONAL JOURNAL OF DAMAGE MECHANICS	2,428	3.988	0.00194
159	Frontiers in Materials	4,309	3.985	0.00583
160	Physical Review Materials	10,814	3.980	0.02792
161	NANOTECHNOLOGY	50,869	3.953	0.03290
162	KONA Powder and Particle Journal	981	3.919	0.00054
163	PHYSICAL REVIEW B	421,250	3.908	0.24025
164	Science China-Technological Sciences	6,731	3.903	0.00599
165	ORGANIC ELECTRONICS	14,558	3.868	0.01250
166	CMC-Computers Materials & Continua	4,859	3.860	0.00359
167	International Journal of Minerals Metallurgy and Materials	4,491	3.850	0.00320
168	INTERNATIONAL JOURNAL OF ADHESION AND ADHESIVES	8,584	3.848	0.00445
169	Advances in Manufacturing	1,340	3.837	0.00126
170	ChemNanoMat	3,269	3.820	0.00448
171	DIAMOND AND RELATED MATERIALS	12,705	3.806	0.00700
172	Road Materials and Pavement Design	6,182	3.805	0.00461
173	Journal of Nanomaterials	13,841	3.791	0.00643
174	FIRE SAFETY JOURNAL	8,175	3.780	0.00439
174	Flexible and Printed Electronics	885	3.768	0.00141

Selected JCR Year: 2021; Selected Categories: "MATERIALS SCIENCE, MULTIDISCIPLINARY"

Rank	Full Journal Title	Total Cites	Journal Impact Factor	Eigenfaktor
174	OPTICAL MATERIALS	21,695	3.754	0.01502
177	Materials	78,439	3.748	0.07693
178	NEW CARBON MATERIALS	1,892	3.700	0.00108
179	Liquid Crystals Reviews	303	3.700	0.00042
180	Materials Today Communications	7,296	3.662	0.00756
181	JOURNAL OF MATERIALS IN CIVIL ENGINEERING	20,492	3.651	0.01344
182	FIRE TECHNOLOGY	3,592	3.605	0.00289
183	MATERIALS LETTERS	60,468	3.574	0.03568
184	COMPUTATIONAL MATERIALS SCIENCE	31,850	3.572	0.02003
185	Green Materials	372	3.564	0.00039
186	International Journal of Mechanics and Materials in Design	1,294	3.561	0.00121
187	JOURNAL OF NUCLEAR MATERIALS	38,379	3.555	0.01690
188	Integrating Materials and Manufacturing Innovation	896	3.551	0.00110
189	PARTICLE & PARTICLE SYSTEMS CHARACTERIZATION	4,148	3.467	0.00315
190	METALS AND MATERIALS INTERNATIONAL	5,091	3.451	0.00389
191	Advances in Production Engineering & Management	627	3.419	0.00052
192	Materials Science and Engineering B-Advanced Functional Solid-State Materials	13,361	3.407	0.00456
193	FATIGUE & FRACTURE OF ENGINEERING MATERIALS & STRUCTURES	7,019	3.373	0.00484
194	MECHANICS OF ADVANCED MATERIALS AND STRUCTURES	4,749	3.338	0.00418
195	Magnetochemistry	988	3.336	0.00120
196	MATERIALS TECHNOLOGY	2,682	3.297	0.00180

Selected JCR Year: 2021; Selected Categories: "MATERIALS SCIENCE, MULTIDISCIPLINARY"

Rank	Full Journal Title	Total Cites	Journal Impact Factor	Eigenfaktor
197	Nanomaterials and Nanotechnology	680	3.280	0.00053
198	Physica Status Solidi-Rapid Research Letters	4,666	3.277	0.00525
199	Beilstein Journal of Nanotechnology	6,636	3.272	0.00568
200	Particuology	4,472	3.251	0.00286
201	Coatings	11,497	3.236	0.01111
202	JOURNAL OF CULTURAL HERITAGE	5,804	3.229	0.00499
203	International Journal of Concrete Structures and Materials	1,827	3.192	0.00172
204	Electronic Materials Letters	1,867	3.151	0.00130
205	Carbon Letters	1,547	3.117	0.00098
206	JOURNAL OF MAGNETISM AND MAGNETIC MATERIALS	45,543	3.097	0.02524
207	Optical Materials Express	8,853	3.074	0.01054
208	Photonics and Nanostructures-Fundamentals and Applications	1,195	3.064	0.00103
209	GRANULAR MATTER	3,770	3.010	0.00334
210	APPLIED PHYSICS A-MATERIALS SCIENCE & PROCESSING	24,130	2.983	0.01402
211	IEEE TRANSACTIONS ON NANOTECHNOLOGY	4,467	2.967	0.00364
212	Silicon	5,320	2.941	0.00412
213	MRS Communications	2,329	2.935	0.00311
214	JOURNAL OF MATERIALS RESEARCH	21,215	2.909	0.00944
215	METALLURGICAL AND MATERIALS TRANSACTIONS B-PROCESS METALLURGY AND MATERIALS PROCESSING SCIENCE	13,007	2.872	0.00622
216	CURRENT APPLIED PHYSICS	8,210	2.856	0.00409

Selected JCR Year: 2021; Selected Categories: “MATERIALS SCIENCE, MULTIDISCIPLINARY”

Rank	Full Journal Title	Total Cites	Journal Impact Factor	Eigenfaktor
217	Heritage Science	1,514	2.843	0.00218
218	Applied Sciences-Basel	63,761	2.838	0.07328
219	EXPERIMENTAL MECHANICS	7,075	2.794	0.00314
220	JOURNAL OF MATERIALS SCIENCE-MATERIALS IN ELECTRONICS	34,378	2.779	0.02870
221	JOURNAL OF INTELLIGENT MATERIAL SYSTEMS AND STRUCTURES	8,879	2.774	0.00537
222	Plasmonics	4,970	2.726	0.00442
223	METALLURGICAL AND MATERIALS TRANSACTIONS A-PHYSICAL METALLURGY AND MATERIALS SCIENCE	37,356	2.726	0.01357
224	MATHEMATICS AND MECHANICS OF SOLIDS	2,331	2.719	0.00348
225	Metals	15,992	2.695	0.01802
226	LIQUID CRYSTALS	6,313	2.676	0.00300
227	Crystals	9,024	2.670	0.01172
228	PROCEEDINGS OF THE INSTITUTION OF MECHANICAL ENGINEERS PART L-JOURNAL OF MATERIALS-DESIGN AND APPLICATIONS	2,205	2.663	0.00162
229	Multidiscipline Modeling in Materials and Structures	922	2.655	0.00090
230	INTERNATIONAL JOURNAL OF FRACTURE	8,695	2.635	0.00280
231	Frontiers of Materials Science	987	2.612	0.00059
232	JOM	15,413	2.597	0.01094
233	Advances in Concrete Construction	1,058	2.580	0.00090
234	JOURNAL OF NANOPARTICLE RESEARCH	15,336	2.533	0.00559
235	JOURNAL OF POROUS MATERIALS	4,193	2.523	0.00255
236	JOURNAL OF LASER APPLICATIONS	2,917	2.521	0.00220

Selected JCR Year: 2021; Selected Categories: "MATERIALS SCIENCE, MULTIDISCIPLINARY"

Publication 3: Straightened Segmentation in 4D Cardiac CT: A Practical Method for Multiparametric Characterization of the Landing Zone for Transcatheter Pulmonary Valve Replacement.

Sun X*****, **Hao Y***, Steitz M, Breitenstein-Attach A, Sebastian Kiekenap JF, Emeis J, Khan MB, Berger F, Schmitt B. Straightened Segmentation in 4D Cardiac CT: A Practical Method for Multiparametric Characterization of the Landing Zone for Transcatheter Pulmonary Valve Replacement. Appl. Sci. 2022, 12, 12912.

https://doi.org/10.3390/app122412912

*Share first authorship.

applied sciences

MDPI

Article

Straightened Segmentation in 4D Cardiac CT: A Practical Method for Multiparametric Characterization of the Landing Zone for Transcatheter Pulmonary Valve Replacement

Xiaolin Sun [1,2,3,†], Yimeng Hao [1,2,†], Marvin Steitz [1,2], Alexander Breitenstein-Attach [1,2], Jonathan Frederik Sebastian Kiekenap [1], Jasper Emeis [1], Mahamuda Badhon Khan [1], Felix Berger [1,2] and Boris Schmitt [1,2,3,4,5,*]

[1] Department of Pediatric Cardiology and Congenital Heart Disease, Charité University Medicine Berlin, Augustenburger Platz 1, 13353 Berlin, Germany
[2] Department of Pediatric Cardiology and Congenital Heart Disease, Deutsches Herzzentrum Berlin, Augustenburger Platz 1, 13353 Berlin, Germany
[3] DZHK (German Centre for Cardiovascular Research), Potsdamer Straße 58, 10785 Berlin, Germany
[4] BIH (Berlin Institute of Health), Anna-Louisa-Karsch-Straße 2, 10178 Berlin, Germany
[5] BCRT (BIH Center of Regenerative Therapies), Föhrer Straße 15, 13353 Berlin, Germany
* Correspondence: schmitt@dhzb.de; Tel.: +49-(0)30-4593-2875
† These authors have contributed equally to this work and share first authorship.

Citation: Sun, X.; Hao, Y.; Steitz, M.; Breitenstein-Attach, A.; Kiekenap, J.F.S.; Emeis, J.; Khan, M.B.; Berger, F; Schmitt, B. Straightened Segmentation in 4D Cardiac CT: A Practical Method for Multiparametric Characterization of the Landing Zone for Transcatheter Pulmonary Valve Replacement. *Appl. Sci.* **2022**, *12*, 12912. https://doi.org/10.3390/app122412912

Academic Editor: Julio Garcia Flores

Received: 18 November 2022
Accepted: 14 December 2022
Published: 15 December 2022

Publisher's Note: MDPI stays neutral with regard to jurisdictional claims in published maps and institutional affiliations.

Featured Application: Four-dimensional cardiac straightened segmentation can be useful for the periprocedural evaluation of TPVR.

Abstract: Cardiac computed tomography angiography (C-CTA) is crucial in assessing the right ventricular outflow tract (RVOT) prior to a transcatheter pulmonary valve replacement (TPVR), as an incorrect evaluation can make the procedure more challenging and can lead to device-related complications. This study aimed to evaluate the feasibility and accuracy of 4D straightened segmentation for a landing zone analysis over anatomical segmentation. Seven pre-operative CTAs and seven post-operative CTAs were used to measure the cross-sectional area, circumference, and diameters at five selected planes as the landing zone for TPVR and compared these to the 4D straightened model with the anatomical model. Furthermore, the right ventricular volume, stent volume, and 4D ellipticity index were calculated from the 4D straightened model. The 4D straightened segmentation had comparable accuracy and efficacy for the measurements at the landing zone. The cross-sectional area and the circumference varied greatly at the RVOT and the basal plane of the pulmonary valve compared with the other three planes of the 4D straightened models from the pre-operative CTAs; however, only the values at the RVOT were found to vary greatly from the post-operative CTAs. The 4D straightened model can provide accurate measurements and is thus a useful method for the periprocedural evaluation of TPVR.

Keywords: four-dimensional computed tomography; transcatheter pulmonary valve replacement; cardiac catheterization; 4D dynamic segmentation; landing zone

1. Introduction

Transcatheter pulmonary valve replacement (TPVR) is a well-established alternative therapeutic approach for patients with right ventricular outflow tract (RVOT) dysfunction, the majority of whom are young and suffer from congenital heart defects or have had multiple previous cardiac surgeries [1,2]. Recent studies show that, in terms of survival and freedom from reintervention or surgery, the outcomes of TPVR are comparable with those of surgical conduit/valve replacement to manage RVOT dysfunction across a

wide age range [3,4]. Similar to transcatheter aortic valve replacement (TAVR), cardiac computed tomography angiography (C-CTA) plays a crucial role in the characterization of the morphology, distensibility, and compliance of the RVOT prior to TPVR, since inaccurate sizing can complicate the procedure and cause device-related complications, such as embolization and paravalvular leak (PVL) [5,6].

Technological developments in three-dimensional (3D) and four-dimensional (4D) C CTA have opened the door to a novel method for the personalized planning of transcatheter heart valve implantation for patients with structural heart valve diseases [7–9]. Cross-sectional imaging with 3D and 4D C-CTA is critical to determine patients' suitability for TPVR; knowledge of RVOT anatomy, the proximity of the left coronary artery to the native pulmonary root, and the distensibility of the RVOT are indispensable for TPVR [10,11]. In addition to this, 3D and 4D C-CTA can support the identification of candidate percutaneous access routes, including the transfemoral, transjugular, and subclavian routes, and answer key anatomical questions. Furthermore, the landing zone—the ideal implantation site for TPVR—can protect the stented pulmonary valve (PV) from PVL, migration, and coronary compression. To create an accurate 4D segmentation of the landing zone anatomy at the RVOT, CT datasets should undergo segmentation where the personalized CT data are assigned to a region of interest to generate the 4D structures in synchronization with the heart rate. A previous study showed that the RVOT's morphology and size can vary significantly throughout the entire cardiac cycle, and so perimeter- and cross-sectional area-based measurements have proven more reliable than PV annulus diameters alone [12]. Additionally, the necessity of 4D C-CTA is emphasized by Gillespie and colleagues, who encourage taking measurements for the landing zone both during end-systole and end-diastole phases [13].

However, in current traditional clinical and preclinical settings, the resulting 4D CT data are frequently transformed into 3D data for manual quantification and visual evaluation, which can only show static information. Furthermore, anatomical 4D segmentations are unable to fully depict the characteristics of the RVOT adjacent to the aortic root during the course of the cardiac cycle, even with 4D information. Yet, the 4D dynamic volumes of the right ventricle, implanted stent, and landing zone, which are crucial for the quantitative interpretation of TPVR, are only partially illustrated by the available data. In addition to the 4D anatomical segmentation, the angle between the RVOT and the main pulmonary artery can cause the measuring lines to not fully align with the landing zone planes (e.g., the annular plane or sinotubular junction plane), which can result in incorrect landing zone measurements. The 2D properties of the STJ plane, the sinus plane and the pulmonary valve annular plane, are defined by three points at each level—the three commissures, the petaline peak of the sinuses, and the nadir of the pulmonary valve—instead of 3D properties, which could lead to inaccurate landing zone measurements. Multi-planar measurements are often employed in clinical practice to assess the RVOT before TPVR, but due to their 3D properties, planes may be positioned incorrectly in anatomical segmentations.

In this study, we exploited a practical approach to performing multiparametric analyses of pre- and post-interventional C-CTA for TPVR in a sheep model by straightening the 4D anatomical segmentations into a 4D straightened segmentation. Our primary objective was to evaluate the feasibility and accuracy of 4D straightened segmentation in comparison to traditional anatomical segmentation, identify its benefits, and explore its potential as a complementary planning tool in TPVR.

2. Materials and Methods

This study included seven adult sheep (Ovis aries), all of which received humane care in compliance with the guidelines of the European and German Societies of Laboratory Animal Science (FELASA, GV-SOLAS). The legal and ethical committee of the Regional Office for Health and Social Affairs in Berlin (LaGeSo) approved the GrOwnValve preclinical trial aiming to conduct transcatheter pulmonary valve replacement from

autologous pericardium with a self-expandable stent in a sheep model (IC14-G 0062/18). The TPVRs were performed at Charité University Hospital of Berlin, Campus Virchow-Klinikum, Research Institute for Experimental Medicine (FEM), while all 4D cardiac CTs were performed at the German Heart Center Berlin.

2.1. Scan Protocol and 4D Cardiac CT Processing

All cardiac CTAs were performed on a Siemens 64-slice dual-source multidetector CT scanner with ECG gating (SOMATOM Definition Flash, Siemens AG, Munchen, Germany). The sheep were scanned in the prone position with standard acquisition technical parameters: a gantry rotation time of 0.33 s, 100–320 mAs per rotation, a 120 kV tube voltage, matrix 256 with a 16-bit depth, a deviation effective X-ray dose of 15.5 ± 11.6 mSv, and a slice thickness of 0.75 mm. CT contrast enhancement was achieved by administering 2–2.5 mL/kg of an iodinated contrast agent at a rate of 5 mL/s. To achieve the ideal synchronization, a bolus tracking method was used for contrast bolus timing in the region of interest on the main pulmonary artery. The 4D cardiac CTA scanning protocol produced 10 continuous frames for the cardiac cycle, from 10% to 100%, with 10% of the RR interval covering the entire cardiac cycle.

2.2. Four-Dimensional Cardiac CT Analysis in 3D Slicer

2.2.1. Segmentations

The CT data of the seven sheep were processed offline using the open-source software 3D Slicer (https://www.slicer.org/ (accessed on 1 March 2022). The 4D anatomical right heart (from the superior vena cava to the end of the main pulmonary artery, without the inferior vena cava) blood pool was segmented using a certain threshold automatically and manually based on each C-CTA by two experienced doctors and optimized manually by a senior expert. The inferior vena cava was not included in this anatomical segmentation due to its low contrast (the contrast agent was administered via the cephalic vein) and the establishment of the subsequent straightened segmentation.

After creating the anatomical segmentation for each 10% of cardiac cycle, the straightened 4D right heart segmentations were created as follows. Two markup points were placed on the top plane of the superior vena cava and the end plane of the main pulmonary artery to construct a centerline for each anatomical segmentation, and then a centerline curve was generated by adding a new markup curve to the segmentation. An output straightened volume was created by executing the "Curved Planar Reformat" operation. This straightened volume was then used to construct a straightened segmentation both automatically and manually. The segmentation for each 10% of the cardiac cycle was obtained using the same methods. The ten 3D straightened segmentations were sequentially concatenated to create a 4D straightened right heart segmentation.

The straightened 4D right heart models were created by adding centerlines and curved planar reformatting to the corresponding anatomical model. Similar steps were used for all segmentations of both the pre-operative C-CTA (pre-CT) and post-operative C-CTA (post-CT). Comprehensive steps for the 4D cardiac CTA analysis were described previously [14].

2.2.2. Multiparametric Measurements of the Landing Zone

Dynamic landing zone measurements, which included cross-sectional area, circumference, maximum diameter, and minimum diameter in the pre-CTs, were taken in five planes at the landing zone: plane 1—RVOT (10 mm below plane 2), plane 2—BPV plane (three hinge points at the nadir of each of the attachments of the PV), plane 3—sinus plane, plane 4—sinotubular junction (STJ) plane, and plane 5—PA plane (10 mm above plane 4). The five planes in the post-CTs were defined as follows: plane 1—RVOT (10 mm below plane 2), plane 2—bottom plane of the stent (BPS) plane, plane 3—middle plane of the stent (MPS) plane, plane 4—top plane of the stent (TPS) plane, and plane 5—PA plane (10

mm above plane 4) (Figure 1). The RV volume was obtained by cutting the right heart segmentations at the tricuspid valve level and at the level of plane 4 both in the anatomical and the straightened segments. The right ventricular ejection fraction (RVEF) can be calculated using the minimum and maximum RV volume. The volume of the landing zone in the pre- (PV volume) and post-CTs (stent volume, SV) was obtained by cutting the right heart segments from plane 1 to plane 5 both in the anatomical and the straightened segments. The rendered stent volume in the post-CTs was created by masking the right heart volume between plane 2 and 4 for the entire cardiac cycle. The ratio between the minimum and maximum diameter in each section was calculated to determine the grade of the elliptical shape (ellipticity index). The correlation between the anatomical model and straightened model was assessed using the Pearson correlation coefficient. We calculated the r value for the Pearson correlation coefficient using Formula (1),then obtained the t value using Formula (2). In the case where the degrees of freedom (d.f.) for r is $n - 2$, the p value can be obtained using the critical values of t for Pearson's r.

$$r = \frac{n\sum x_i y_i - \sum x_i \sum y_i}{\sqrt{n\sum x_i^2 - (\sum x_i)^2}\sqrt{n\sum y_i^2 - (\sum y_i)^2}} \quad (1)$$

$$t = \frac{r}{\sqrt{\frac{1-r^2}{n-2}}} \quad (2)$$

Bland–Altman analysis was conducted to further confirm the agreement between the two models.

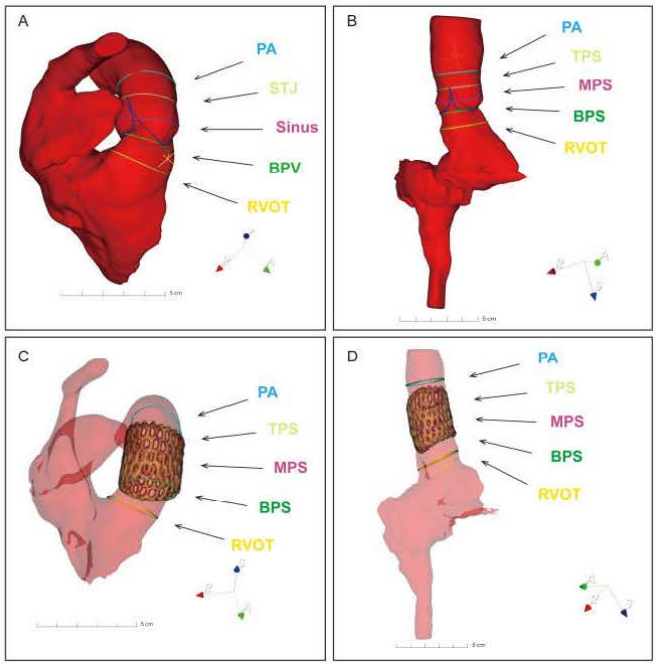

Figure 1. Five selected planes from different segmentations. (**A**) anatomical model from pre-operative CT, (**B**) straightened model from pre-operative CT, (**C**) anatomical model from post-CT, (**D**) straightened model from post-CT. PA pulmonary artery, STJ sinotubular junction, BPV basal plane

of pulmonary valve, RVOT right ventricular outflow tract, TPS top plane of the stent, MPS middle plane of the stent, BPS bottom plane of the stent.

2.3. TPVR Protocol

The sheep were tranquilized with an intramuscular injection of 0.4 mg/kg of midazolam, 0.4 mg/kg of butorphanol, and 0.011 mg/kg of glycopyrronium bromide. After administering intravenous anesthesia by injecting 1–2.5 mg/kg of propofol and 0.01 mg/kg of fentanyl, the sheep were intubated, and a gastric tube was placed into the stomach for gas and fluid evacuation during the preparation for CT and TPVR.

The sheep were ventilated under general anesthesia, which was maintained by isoflurane (1%) in oxygen (flow = 1 L/min, FiO2 = 75%), combined with a continuous rate infusion of fentanyl (5–15 mcg/kg/h) and midazolam (0.2–0.5 mg/kg/h) during the left mini-thoracotomy to harvest the autologous pericardium and perform the transjugular implantation of the autologous heart valve. GrOwnValve sizing was achieved according to the 4D measurements of the landing zone in the pre-CTs (Figure 1A). The autologous pericardium was harvested to manufacture a new PV by trimming and sewing it onto a Nitinol stent. The stented autologous PVs were loaded into the head of a self-designed delivery system and advanced via the left jugular vein under guidewire and fluoroscopy guidance. After confirmation of the deployment position in the right heart angiography, the GrOwnValve was deployed at the native PV position. The protocol for the GrOwnValve transjugular vein implantation was illustrated in detail previously [15].

2.4. Statistical Analysis

Statistics were analyzed using the GraphPad Prism 9 software (Graphpad Software, Biomatters, Ltd., NZ, and GSL Biotech, San Diego, CA, USA). Normal distribution was assessed with a Kolmogorov–Smirnov test. Continuous variables are presented as mean ± standard deviation (SD) for normal distribution or as median with interquartile ranges (IQRs) for non-normal distribution. The Pearson correlation coefficient was used to quantify the correlation between each plane of the anatomical model and the straightened model during the ten cardiac phases for each of the seven sheep. The agreement and bias between the two models were assessed with Bland–Altman analysis. A p value of < 0.05 was considered statistically significant. All the test results are two-tailed.

3. Results

3.1. Four-Dimensional Cardiac CT Segmentation

Fourteen C-CTA datasets (a pre-CT and a post-CT from each of the seven sheep) were included in the study. Each CT was divided into ten cardiac phases. Furthermore, each CT was reconstructed into an anatomical model and a straightened model. In total, 28 anatomical models and straightened models were successfully segmented and reconstructed from the 14 CTs. The cross-sectional area, circumference, maximum diameter, and minimum diameter of the five planes were measured for each model. This resulted in a total of 350 paired datasets in each measurement that were acquired at the 10 different cardiac cycles between the anatomical model and the straightened model. In addition, the parameters for a single plane were compared as well.

3.2. Correlations between Anatomical Model and Straightened Model

In all pre-CT comparisons, there was a strong linear correlation between the anatomical model and the straightened model for the cross-sectional area and the circumference measurements at all five planes, with a Pearson correlation coefficient of 0.95 ($p < 0.0001$) for the cross-sectional area and 0.94 ($p < 0.0001$) for the circumference. The Bland–Altman analysis further confirmed a strong agreement between the two models (Figure 2).

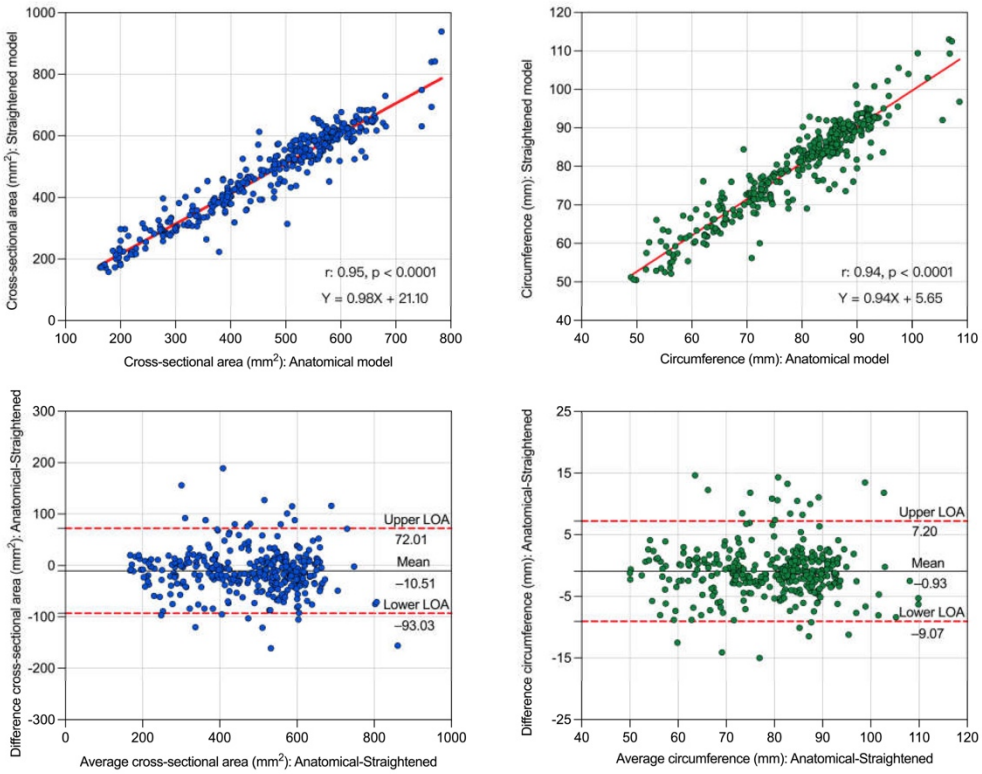

Figure 2. Pearson correlation scatterplot and Bland–Altman plot of cross-sectional area and circumference for the agreement between the anatomical model and straightened model from pre-CT. LOA—limit of agreement.

Similarly, the two pre-CT models for the minimum and maximum diameter were highly correlated, with a Pearson correlation coefficient of 0.96 ($p < 0.0001$) for the minimum diameter and 0.91 ($p < 0.0001$) for the maximum diameter. The limits of agreement between the anatomical model and the straightened model were in a good range for both the minimum diameter and maximum diameter (Figure 3).

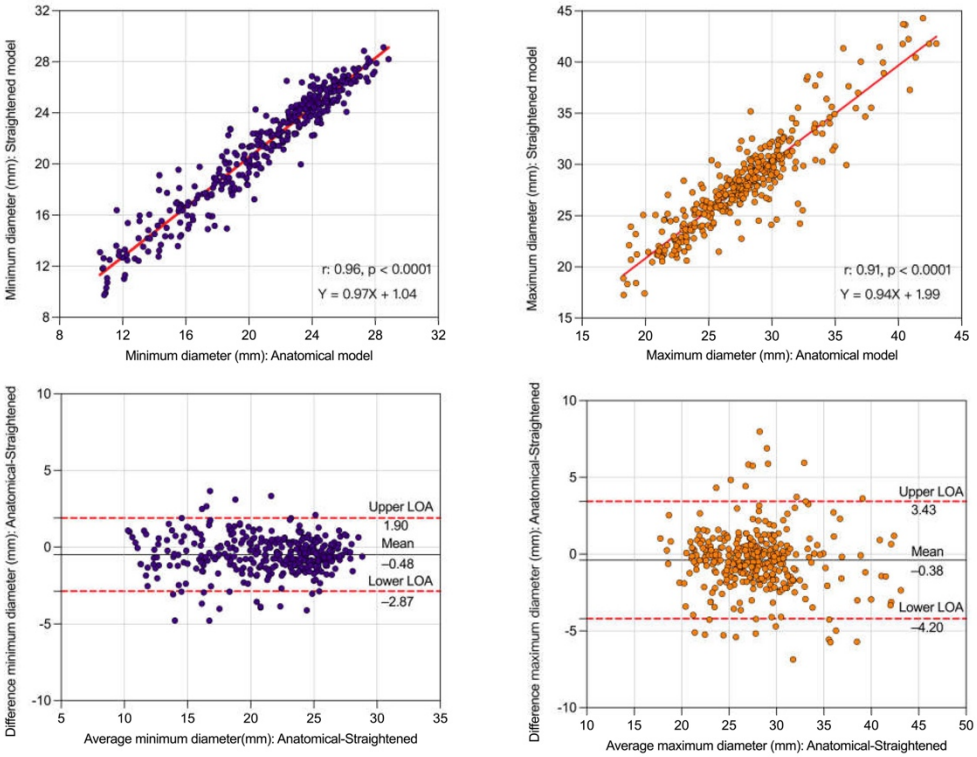

Figure 3. Pearson correlation scatterplot and Bland–Altman plot of minimum diameter and maximum diameter for the agreement between anatomical model and straightened model from pre-CT. LOA—limit of agreement.

There was also a statistically significant linear correlation between the cross-sectional area (r: 0.97, $p < 0.0001$) and the circumference (r: 0.97, $p < 0.0001$) of the two models for the post-CTs (Figure 4). The scatter plot of the Bland–Altman analysis also demonstrates good agreement for every paired dataset.

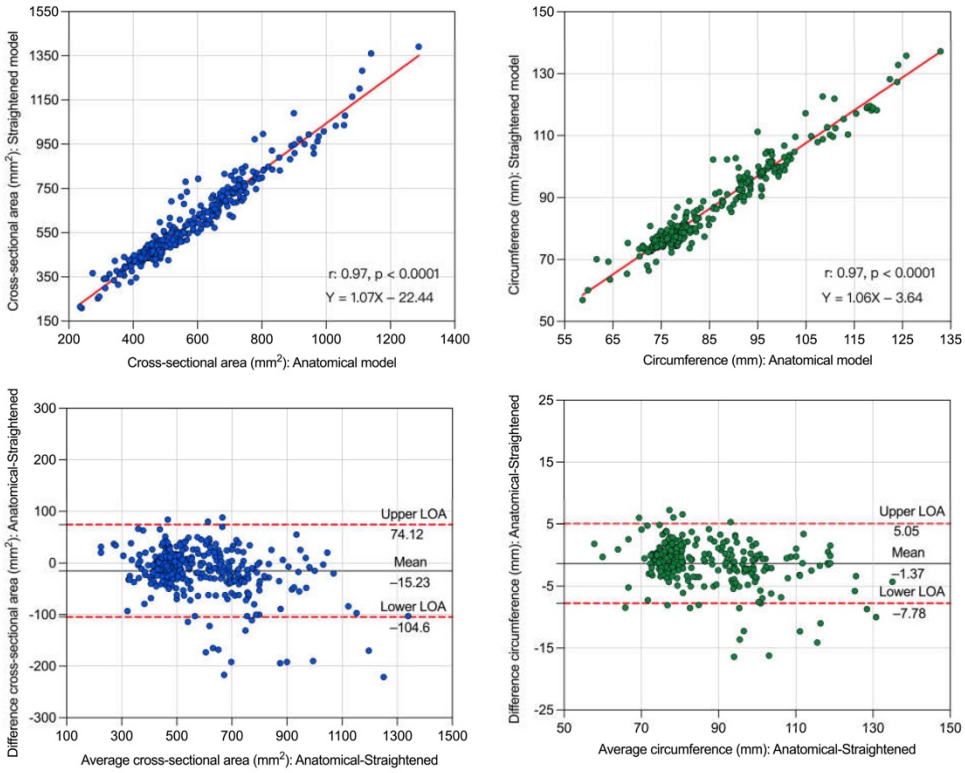

Figure 4. Pearson correlation scatterplot and Bland–Altman plot of cross-sectional area and circumference for the agreement between the anatomical model and straightened model from post-CT. LOA—limit of agreement.

The post-CT anatomical model and straightened model for the minimum diameter and maximum diameter were highly correlated, with a Pearson correlation coefficient of 0.96 ($p < 0.0001$) for the minimum diameter and 0.91 ($p < 0.0001$) for the maximum diameter. The limits of agreement between the anatomical model and the straightened model were in a good range (Figure 5).

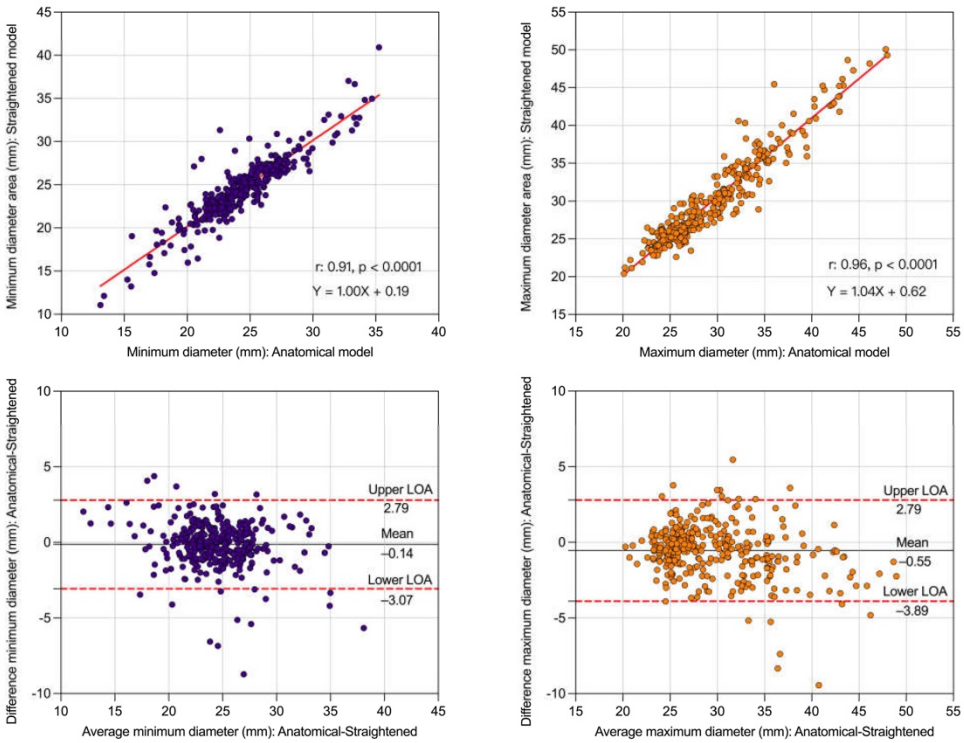

Figure 5. Pearson correlation scatterplot and Bland–Altman plot of minimum diameter and maximum diameter for the agreement between the anatomical model and straightened model from post-CT. LOA—limit of agreement.

The Pearson correlation coefficients and Bland–Altman agreements between the two model measurements of the annulus area, circumference, minimum diameter, and maximum diameter at each single plane are shown in Table 1. There was also an excellent correlation between every comparison. The results for the Pearson correlation coefficients and Bland–Altman analyses indicate a good accuracy of the straightened model.

Table 1. Pearson correlation coefficient and Bland–Altman analysis of cross-sectional area, circumference, minimum diameter, and maximum diameter for each single plane. CSA—cross-sectional area, C—circumference, LOA—limit of agreement, RVOT—right ventricular outflow tract, BPV—basal plane of pulmonary valve, STJ—sinotubular junction, PA—pulmonary artery, BPS—bottom plane of the stent, MPS—middle plane of the stent, TPS—top plane of the stent. * $p < 0.0001$.

Pre-CT		Pearson Correlation (r)	Bland–Altman Analysis		
			Mean Difference	Upper LOA	Lower LOA
RVOT	CSA (mm^2)	0.96 *	−7.43	95.24	−110.10
	C (mm)	0.95 *	−0.23	10.05	−10.51
	Minimum diameter (mm)	0.94 *	−0.49	2.32	−3.31
	Maximum diameter (mm)	0.94 *	−0.54	4.05	−5.13
BPV	CSA (mm^2)	0.87 *	−4.89	117.60	−127.40
	C (mm)	0.84 *	−0.89	12.23	−14.01

	Minimum diameter (mm)	0.88 *	−0.49	2.94	−3.92
	Maximum diameter (mm)	0.77 *	−0.18	6.03	−6.40
Sinus	CSA (mm²)	0.93 *	−5.00	54.53	−64.53
	C (mm)	0.94 *	−0.87	4.03	−5.76
	Minimum diameter (mm)	0.92 *	−0.34	1.29	−1.98
	Maximum diameter (mm)	0.90 *	−0.13	1.79	−2.04
STJ	CSA (mm²)	0.97 *	−14.30	30.54	−59.14
	C (mm)	0.97 *	−1.02	2.68	−4.72
	Minimum diameter (mm)	0.93 *	−0.61	1.15	−0.61
	Maximum diameter (mm)	0.94 *	−0.35	1.49	−2.18
PA	CSA (mm²)	0.97 *	−20.94	29.80	−71.68
	C (mm)	0.97 *	−1.67	2.24	−5.57
	Minimum diameter (mm)	0.95 *	−0.48	1.29	−2.25
	Maximum diameter (mm)	0.92 *	−0.73	1.71	−3.17
RVOT	CSA (mm²)	0.97 *	−37.39	110.10	−184.90
	C (mm)	0.97 *	−2.70	7.53	−12.92
	Minimum diameter (mm)	0.91 *	−0.40	4.94	−5.73
	Maximum diameter (mm)	0.93 *	−1.47	3.52	−6.46
BPS	CSA (mm²)	0.95 *	0.96	67.47	−65.55
	C (mm)	0.95 *	0.13	5.44	−5.17
	Minimum diameter (mm)	0.84 *	0.05	2.11	−2.00
	Maximum diameter (mm)	0.93 *	0.06	2.73	−2.61
MPS	CSA (mm²)	0.99 *	−10.36	23.76	−44.47
	C (mm)	0.99 *	−0.78	1.87	−3.43
	Minimum diameter (mm)	0.92 *	−0.19	1.29	−1.67
	Maximum diameter (mm)	0.96 *	−0.24	1.49	−1.96
TPS	CSA (mm²)	0.97 *	−21.57	42.77	−85.91
	C (mm)	0.97 *	−1.74	3.26	−6.75
	Minimum diameter (mm)	0.93 *	0.11	1.92	−1.70
	Maximum diameter (mm)	0.97 *	−0.9	1.67	−3.47
PA	CSA (mm²)	0.97 *	−7.77	66.30	−81.84
	C (mm)	0.97 *	−0.40	5.57	−6.38
	Minimum diameter (mm)	0.92 *	−0.27	1.85	−2.39
	Maximum diameter (mm)	0.94 *	−0.18	2.77	−3.13

3.3. Dynamic Variation of Landing Zone

The mean cross-sectional area and circumference dynamic variations of each plane during the whole cardiac cycle for the pre- and the post-CTs are shown in Figures 6 and 7. There was high variation in the RVOT and BPV cross-sectional area for the pre-CTs in the ten phases of the cardiac cycle, especially from 50% to 60% and 90% to 100%. For the straightened pre-CT model, the maximum and minimum mean annulus areas of the RVOT plane were 646 ± 149 mm² (90%) and 272 ± 122 mm² (50%), respectively, and the maximum and minimum cross-sectional area mean values of the BPV plane were 471 ± 48 mm² (100%) and 266 ± 101 mm² (60%), respectively. In addition, the post-CT RVOT annulus area differed greatly between 100% and 50% with areas of 1028 ± 210 mm² and 435 ± 144 mm², respectively. The dynamic variation trends for the circumference were similar to those for the cross-sectional area. The detailed mean differences (±standard deviation) of the cross-sectional area and the circumference are presented in Table S1. However, the variation in the BPS plane area in the post-CTs was small because the radial force of the implanted stent fixed the stent on the annulus between the BPS and the PA plane, allowing the PA to expand fully, which also led to an increase in the annulus ellipticity of the BPS plane (Table 2). The annulus of the RVOT plane has a more notable elliptical geometry

than the other planes. The detailed ellipticity indices of the five planes during the ten cardiac phases are presented in Table S2.

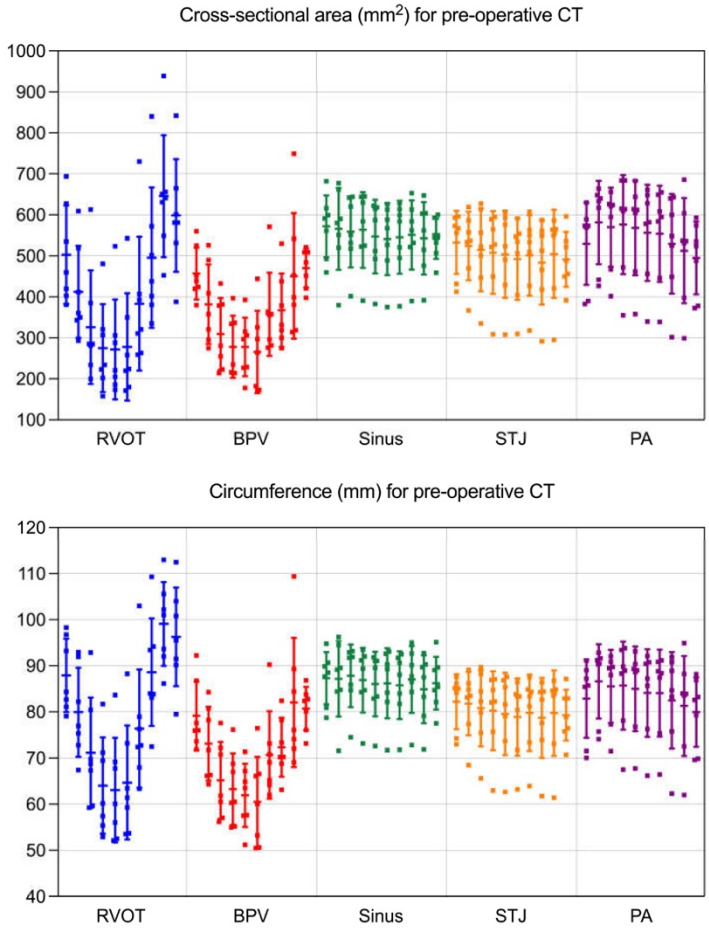

Figure 6. Dynamic variation in the cross-sectional area and circumference throughout the cardiac cycle at five planes from pre-operative CT. RVOT—right ventricular outflow tract, BPV—basal plane of pulmonary valve, STJ—sinotubular junction, PA—pulmonary artery. In each plane, one error bar indicates one frame (from 10% to 100%) in the cardiac cycle.

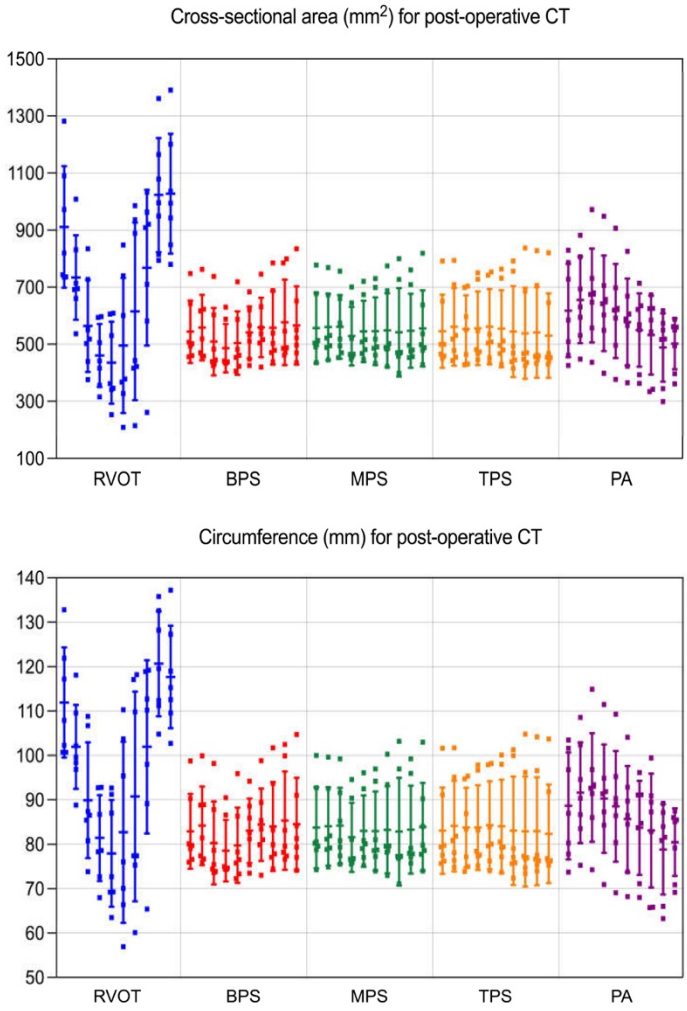

Figure 7. Dynamic variation in the cross-sectional area and circumference throughout the cardiac cycle at five planes from post-operative CT. RVOT—right ventricular outflow tract, BPS—bottom plane of the stent, MPS—middle plane of the stent, TPS—top plane of the stent, PA—pulmonary artery. In each plane, one error bar indicates one frame (from 10% to 100%) in the cardiac cycle.

Table 2. Annulus ellipticity index of five planes for pre-operative CT and post-operative CT. The ellipticity index was defined as minimum diameter/maximum diameter.

Ellipticity Index			
Pre-CT		**Post-CT**	
RVOT	0.55 ± 0.08	RVOT	0.69 ± 0.10
BPV	0.69 ± 0.12	BPS	0.88 ± 0.08
Sinus	0.89 ± 0.06	MPS	0.88 ± 0.09
STJ	0.90 ± 0.06	TPS	0.84 ± 0.10
PA	0.83 ± 0.06	PA	0.86 ± 0.09

4. Discussion

In this study, we illustrated the feasibility and accuracy of multiparametric analyses of the landing zone using 4D straightened segmentation generated from 4D C-CTA in sheep to measure and characterize the dynamic changes in the landing zone in pre-CTs and the implanted stent in post-CTs for TPVR at five selected planes. Furthermore, we used this methodology to obtain the 4D RV volume from all CTs, the landing zone volume from pre-CTs, the stent volume from post-CTs, and the ellipticity index at the selected planes, all of which could be used to estimate the right heart function, new heart valve selection, stent conditions following TPVR, and to help us gain a better understanding of the deformation of the landing zone at the native RVOT. Finally, we determined the differences in the cross-sectional area and perimeter on the selected pulmonary artery plane and the RVOT plane by comparing the corresponding pre- and post-CTs, thus reflecting the structural changes after TPVR. Compared with anatomical 4D segmentation, this straightened model not only has the comparable accuracy of relative measurement, but it also aids in better understanding the deformation of the landing zone at the native RVOT and the implanted stent, while supporting the development of new TPVR devices that are not only morphologically appropriate for the majority of patients scheduled to undergo TPVR, but also achieve better mechanical performance in the long term. Additionally, this straightened 4D segmentation aids in determining proper valve sizing by measuring the parameters in the appropriate planes.

Methods involving 3D echocardiography, fluoroscopy imaging, and 3D C-CTA are usually employed to evaluate cross-sectional changes at the RVOT, which are based on 3D alignment and fixed-plane segmentation [16–18]. Currently, 4D C-CTA can measure and characterize the changes in heart morphology and size throughout the cardiac cycle [19]. However, the current method for 4D segmentation is based on anatomical right heart reconstruction, which can neither fully describe the features of the RVOT-PA nor reveal intuitive observations. Furthermore, there is no method to quantify the RVOT-PA using comprehensive 4D C-CTA analysis. Along with the 4D anatomical segmentation, the angle between the RVOT and the main pulmonary artery may prevent the measuring lines from perfectly aligning with the planes of the landing zone (such as the annular plane and the sinotubular junction plane, which are extremely important for TPVR), which could lead to inaccurate landing zone measurements. Additionally, as the landing zone for TPVR is not a straight conduit, this could increase the difficulty of placing the planes in the right position, as well as the measurements. In clinical practice, it is crucial to obtain the precise length of the TPVR landing zone to avoid right and/or left pulmonary artery occlusion when adapting a self-expandable stented heart valve. In addition, in the landing zone for TPVR, only the RVOT plane and main pulmonary artery plane are the "real 2D flat planes." The other three planes, STJ, sinus, and the basal plane of the pulmonary valve, are defined by three points (STJ—the three commissures; sinus—the three peaks of the sinuses; and the basal plane of the pulmonary valve—the nadir of the pulmonary valve). These three planes are virtual planes, or at least not 2D flat planes; they are characterized by 3D features. Even multi-planar measurements are widely used in clinical practice to evaluate the RVOT prior to TPVR, but planes could be placed inaccurately in anatomical segmentations due to their 3D features and the angle of observation. In this study, we applied a 4D straightened segmentation with comparable accuracy and efficacy for five planar measurements from seven pre-CTs and seven post-CTs, which not only illustrates and visualizes the right heart's total deformation throughout the cardiac cycle but also quantitatively characterizes the RVOT as a whole. All measurements at the necessary planes can be easily checked using this 4D straightened segmentation. The cross-sectional area, circumference, and max–min diameters measured from the 4D straightened models show a strong linear correlation and strong agreement with the 4D anatomical models. With the 4D straightened models from the pre-CTs, the cross-sectional area and circumference were found to vary greatly at the RVOT and the BPV compared with the other three planes, which is consistent with anatomical measurements from a previous study

[12]; however, only the values at the RVOT were found to vary greatly from those derived from the post-CTs.

It is evident that single parameters alone are unable to reflect the features of the right heart clearly and comprehensively. Therefore, multiple parameters are needed to enable adequate pre- and post-TPVR evaluation of the right heart. Conventionally, cardiac function is assessed by 2D/3D echocardiography and cardiac magnetic resonance imaging (MRI) and is based mainly on the left ventricular ejection fraction (LVEF) and not the RVEF [20,21]. Furthermore, the RV volume cannot be evaluated precisely by echocardiography during clinical application due to the patient's complex anatomy after open-heart surgery and the influence of breathing. In order to address this issue and improve the evaluation, RV volume should be estimated by multiple parameters. In this context, 4D RV volume measurements from 4D C-CTA could play an important role. We successfully segmented and calculated 4D RV volume from pre- and post-CT (Table S1) to measure the distance between the right ventricular inflow tract and the RVOT, which allowed for the innovation of the delivery system and the planning of the access route for TPVR according to the length of the delivery system from pre-CT, evaluating the RVEF perioperatively. In addition, for the pre- and post-TPVR evaluation, we defined volume among the five dynamic planes as our specific landing zone for our self-designed TPVR device and quantitatively measured the volume deformation throughout the entire cardiac cycle to obtain directly perceived motions, such as the dynamics of the landing zone volume, the implanted stent volume, and the native PV volume (Table S1). Two of the enrolled sheep (sheep F and J) were selected for a representative illustration of the 4D dynamic segmentation (Videos S1–S8). Additionally, calculating the 4D ellipticity index of the implanted stent allowed us to easily observe the stent deformations during the cardiac cycle and evaluate the stented valve size.

The morphology of the implanted stent after full deployment is crucial for the new heart valve to function. Improper morphology of the implanted stent could give rise to a paravalvular leak or new heart valve regurgitation and could result in an inefficient opening area, which could lead to poor long-term performance [9,11,22]. In order to prevent the improper morphology of the implanted stent, a better understanding of the anatomy and device innovation are critical. We calculated the 4D ellipticity index of the landing zone from pre- and post-CT, which showed a lower ellipticity index at the RVOT and the BPV planes compared with the three other planes from pre-CT, while only the RVOT had a lower ellipticity index in post-CT because of the fixation of the implanted stent. The oval geometry of the BPV is an indicator of whether patients will benefit from TPVR because the myocardium at the BPV level would squeeze the stent into an undesirable geometry during the systolic phase, which could lead to an inefficient opening area in the new heart valve. The changes in the cross-sectional area and circumference during the cardiac cycle should also be taken into account for proper valve sizing, which is conventionally performed within 3D C-CTA by selecting the end-diastolic phase. However, based on the results of our study, it may be more expedient to select the mid-systolic phase for valve sizing because the largest cross-sectional area and circumference at the BPV and the STJ could prevent an elliptical geometry in the implanted stent. Additionally, a comprehensive evaluation of the "neighborhood" surrounding the left coronary artery is required. This could also encourage medical engineers to develop elliptical stents and heart valves with new features.

This study has several limitations. First, the accuracy and feasibility of the 4D straightened model were only demonstrated with seven pre-CTs and seven post-CTs, and need to be further proven with a larger population. Additionally, all pre-CTs were obtained from healthy sheep without any congenital heart defects. For clinical application, especially in patients who have undergone transannular patch repair/Ross procedures or other open-heart surgeries, additional work would be required to reconstruct the heart's architecture due to artifacts from adhesions between the pericardium and the myocardium, the stent, and the distorted anatomy. To our knowledge, two major artefacts that

significantly affect CT imaging accuracy are the blooming artefact and cardiac movement artefact [23,24]. With technical innovation, by reducing image noises and blooming artefacts, iterative reconstruction (IR) algorithms have the potential to enhance the quality of CT images. Compared to in vivo data, imaging data created from patient-specific models could provide accurate patient-specific geometry parameters without motion artefacts. However, in future studies, the acquisition times and contrast resolutions of scanners still need to be improved to obtain higher accuracy in CT imaging, which would improve the evaluation of TPVR outcomes.

5. Conclusions

Four-dimensional straightened segmentation can be a useful method for periprocedural evaluations for TPVR and could assist TPVR device innovation in the future.

6. Patents

There is no patent resulting from the work reported in this manuscript.

Supplementary Materials: The following supporting information can be downloaded at https://www.mdpi.com/article/10.3390/app122412912/s1, Table S1: The mean value of parameters for each plane during the cardiac cycle; Table S2: Ellipticity index for each plane during the cardiac cycle; Video S1: The deformation of 4D reconstructed anatomical segmentation from sheep F's pre-CT. Anterior view of the anatomical 4D segmentation with landing zone markers at the five selected planes, 1–6 s. Posterior view of the anatomical 4D segmentation with landing zone markers at the five selected planes, 6–13 s. Superior view of the anatomical 4D segmentation with landing zone markers at the five selected planes, 13–19 s; Video S2: The deformation of 4D reconstructed straightened segmentation from sheep F's pre-CT. Anterior view of the straightened 4D segmentation with landing zone markers at the five selected planes, 1–6 s. Posterior view of the straightened 4D segmentation with landing zone markers at the five selected planes, 6–13 s. Superior view of the straightened 4D segmentation with landing zone markers at the five selected planes, 13–19 s; Video S3: The deformation of 4D reconstructed anatomical segmentation from sheep F's post-CT. Anterior view of the anatomical 4D segmentation with landing zone markers at the five selected planes (with/without the implanted stent), 1–23 s. Posterior view of the anatomical 4D segmentation with landing zone markers at the five selected planes (with/without the implanted stent), 23–46 s. Superior view of the anatomical 4D segmentation with landing zone markers at the five selected planes (with/without the implanted stent), 46–69 s; Video S4: The deformation of 4D reconstructed straightened segmentation from sheep F's post-CT. Anterior view of the straightened 4D segmentation with landing zone markers at the five selected planes (with/without the implanted stent), 1–12 s. Posterior view of the straightened 4D segmentation with landing zone markers at the five selected planes (with/without the implanted stent), 12–24 s. Superior view of the straightened 4D segmentation with landing zone markers at the five selected planes (with/without the implanted stent), 24–37 s; Video S5: The deformation of 4D reconstructed anatomical segmentation from sheep J's pre-CT. Anterior view of the anatomical 4D segmentation with landing zone markers at the five selected planes, 1–6 s. Posterior view of the anatomical 4D segmentation with landing zone markers at the five selected planes, 6–13 s. Superior view of the anatomical 4D segmentation with landing zone markers at the five selected planes, 13–19 s; Video S6: The deformation of 4D reconstructed straightened segmentation from sheep J's pre-CT. Anterior view of the straightened 4D segmentation with landing zone markers at the five selected planes, 1–6 s. Posterior view of the straightened 4D segmentation with landing zone markers at the five selected planes, 6–13 s. Superior view of the straightened 4D segmentation with landing zone markers at the five selected planes, 13–20 s; Video S7: The deformation of 4D reconstructed anatomical segmentation from sheep J's post-CT. Anterior view of the anatomical 4D segmentation with landing zone markers at the five selected planes (with/without the implanted stent), 1–13 s. Posterior view of the anatomical 4D segmentation with landing zone markers at the five selected planes (with/without the implanted stent), 13–25 s. Superior view of the anatomical 4D segmentation with landing zone markers at the five selected planes (with/without the implanted stent), 25–38 s; Video S8: The deformation of 4D reconstructed straightened segmentation from sheep J's post-CT. Anterior view of the straightened 4D segmentation with landing zone markers at the five selected planes (with/without the implanted stent), 1–12 s. Posterior view of the straightened 4D segmentation with landing zone markers at the five selected planes (with/without

the implanted stent), 12–24 s. Superior view of the straightened 4D segmentation with landing zone markers at the five selected planes (with/without the implanted stent), 24–37 s.

Author Contributions: Conceptualization, X.S., Y.H. and B.S.; methodology, X.S., Y.H. and B.S.; validation, X.S., Y.H. and B.S.; formal analysis, Y.H. and B.S.; investigation, X.S., Y.H., M.S., A.B.-A., J.F.S.K., J.E., M.B.K., F.B. and B.S.; resources, X.S., Y.H., M.S., A.B.-A., J.F.S.K., J.E., M.B.K., F.B. and B.S.; data curation, Y.H.; writing—original draft preparation, X.S., Y.H. and B.S.; writing—review and editing, Y.H., F.B. and B.S.; visualization, X.S., Y.H., M.S., A.B.-A., J.F.S.K., J.E., M.B.K., F.B. and B.S.; supervision, B.S. and F.B.; project administration, X.S., Y.H. and B.S.; funding acquisition, B.S. All authors have read and agreed to the published version of the manuscript.

Funding: This research was funded by from the German Federal Ministry for Economic Affairs and Energy, EXIST—Transfer of Research (03EFIBE103). Xiaolin Sun and Yimeng Hao are supported by the China Scholarship Council (Xiaolin Sun-CSC: 201908080063, Yimeng Hao-CSC: 202008450028). Xiaolin Sun is supported by a doctoral scholarship from Deutsches Zentrum für Herz-Kreislauf-Forschung (DZHK) e.V.

Institutional Review Board Statement: The animal study protocol, involving transcatheter pulmonary valve replacement from autologous pericardium with a self-expandable stent in a sheep model, was approved by the Ethics Committee of the Regional Office for Health and Social Affairs in Berlin (LaGeSo) (protocol code: IC14 g 0062/18, date of approval: 16 August 2018).

Informed Consent Statement: Not applicable.

Data Availability Statement: The data presented in this study are available in Supplementary Material.

Acknowledgments: We extend our heartfelt appreciation to all who contributed to this work, both past and present members. This work is supported by DZHK (German Center for Cardiovascular Research) and the grants from the German Federal Ministry for Economic Affairs and Energy, EXIST—Transfer of Research (03EFIBE103). Xiaolin Sun and Yimeng Hao are supported by the China Scholarship Council (Xiaolin Sun-CSC: 201908080063, Yimeng Hao-CSC: 202008450028). Xiaolin Sun is supported by a doctoral scholarship from DZHK (German Center for Cardiovascular Research).

Conflicts of Interest: The authors declare no conflicts of interest.

References

1. Bonhoeffer, P.; Boudjemline, Y.; Saliba, Z.; Merckx, J.; Aggoun, Y.; Bonnet, D.; Acar, P.; Le Bidois, J.; Sidi, D.; Kachaner, J. Percutaneous replacement of pulmonary valve in a right-ventricle to pulmonary-artery prosthetic conduit with valve dysfunction. *Lancet* **2000**, *356*, 1403–1405. https://doi.org/10.1016/s0140-6736(00)02844-0.
2. Georgiev, S.; Ewert, P.; Eicken, A.; Hager, A.; Hörer, J.; Cleuziou, J.; Meierhofer, C.; Tanase, D. Munich Comparative Study: Prospective Long-Term Outcome of the Transcatheter Melody Valve Versus Surgical Pulmonary Bioprosthesis With Up to 12 Years of Follow-Up. *Circ. Cardiovasc. Interv.* **2020**, *13*, e008963. https://doi.org/10.1161/circinterventions.119.008963.
3. McElhinney, D.B.; Zhang, Y.; Aboulhosn, J.A.; Morray, B.H.; Biernacka, E.K.; Qureshi, A.M.; Torres, A.J.; Shahanavaz, S.; Goldstein, B.H.; Cabalka, A.K.; et al. Multicenter Study of Endocarditis After Transcatheter Pulmonary Valve Replacement. *J. Am. Coll. Cardiol.* **2021**, *78*, 575–589. https://doi.org/10.1016/j.jacc.2021.05.044.
4. McElhinney, D.B.; Zhang, Y.; Levi, D.S.; Georgiev, S.; Biernacka, E.K.; Goldstein, B.H.; Shahanavaz, S.; Qureshi, A.M.; Cabalka, A.K.; Bauser-Heaton, H.; et al. Reintervention and Survival After Transcatheter Pulmonary Valve Replacement. *J. Am. Coll. Cardiol.* **2022**, *79*, 18–32. https://doi.org/10.1016/j.jacc.2021.10.031.
5. Chatterjee, A.; Bajaj, N.S.; McMahon, W.S.; Cribbs, M.G.; White, J.S.; Mukherjee, A.; Law, M.A. Transcatheter Pulmonary Valve Implantation: A Comprehensive Systematic Review and Meta-Analyses of Observational Studies. *J. Am. Heart Assoc.* **2017**, *6*, e006432. https://doi.org/10.1161/jaha.117.006432.
6. Rinaldi, E.; Sadeghi, S.; Rajpal, S.; Boe, B.A.; Daniels, C.; Cheatham, J.; Sinha, S.; Levi, D.S.; Aboulhosn, J. Utility of CT Angiography for the Prediction of Coronary Artery Compression in Patients Undergoing Transcatheter Pulmonary Valve Replacement. *World J. Pediatr. Congenit. Heart Surg.* **2020**, *11*, 295–303. https://doi.org/10.1177/2150135120905670.
7. Elattar, M.A.; Vink, L.W.; van Mourik, M.S.; Baan, J., Jr.; vanBavel, E.T.; Planken, R.N.; Marquering, H.A. Dynamics of the aortic annulus in 4D CT angiography for transcatheter aortic valve implantation patients. *PLoS ONE* **2017**, *12*, e0184133. https://doi.org/10.1371/journal.pone.0184133.
8. Ooms, J.F.; Wang, D.D.; Rajani, R.; Redwood, S.; Little, S.H.; Chuang, M.L.; Popma, J.J.; Dahle, G.; Pfeiffer, M.; Kanda, B.; et al. Computed Tomography-Derived 3D Modeling to Guide Sizing and Planning of Transcatheter Mitral Valve Interventions. *JACC Cardiovasc. Imaging* **2021**, *14*, 1644–1658. https://doi.org/10.1016/j.jcmg.2020.12.034.

9. Pluchinotta, F.R.; Sturla, F.; Caimi, A.; Giugno, L.; Chessa, M.; Giamberti, A.; Votta, E.; Redaelli, A.; Carminati, M. 3-Dimensional personalized planning for transcatheter pulmonary valve implantation in a dysfunctional right ventricular outflow tract. *Int. J. Cardiol.* **2020**, *309*, 33–39. https://doi.org/10.1016/j.ijcard.2019.12.006.
10. Chung, R.; Taylor, A.M. Imaging for preintervention planning: Transcatheter pulmonary valve therapy. *Circ. Cardiovasc. Imaging* **2014**, *7*, 182–189. https://doi.org/10.1161/circimaging.113.000826.
11. Curran, L.; Agrawal, H.; Kallianos, K.; Kheiwa, A.; Lin, S.; Ordovas, K.; Mahadevan, V.S. Computed tomography guided sizing for transcatheter pulmonary valve replacement. *Int. J. Cardiol. Heart Vasc.* **2020**, *29*, 100523. https://doi.org/10.1016/j.ijcha.2020.100523.
12. Schievano, S.; Capelli, C.; Young, C.; Lurz, P.; Nordmeyer, J.; Owens, C.; Bonhoeffer, P.; Taylor, A.M. Four-dimensional computed tomography: A method of assessing right ventricular outflow tract and pulmonary artery deformations throughout the cardiac cycle. *Eur. Radiol.* **2011**, *21*, 36–45. https://doi.org/10.1007/s00330-010-1913-5.
13. Gillespie, M.J.; Benson, L.N.; Bergersen, L.; Bacha, E.A.; Cheatham, S.L.; Crean, A.M.; Eicken, A.; Ewert, P.; Geva, T.; Hellenbrand, W.E.; et al. Patient Selection Process for the Harmony Transcatheter Pulmonary Valve Early Feasibility Study. *Am. J. Cardiol.* **2017**, *120*, 1387–1392. https://doi.org/10.1016/j.amjcard.2017.07.034.
14. Sun, X.; Hao, Y.; Sebastian Kiekenap, J.F.; Emeis, J.; Steitz, M.; Breitenstein-Attach, A.; Berger, F.; Schmitt, B. Four-Dimensional Computed Tomography-Guided Valve Sizing for Transcatheter Pulmonary Valve Replacement. *Thorac. Cardiovasc. Surg.* **2022**, *70*, S67–S103. https://doi.org/10.3791/63367.
15. Hao, Y.; Sun, X.; Kiekenap, J.F.S.; Emeis, J.; Steitz, M.; Breitenstein-Attach, A.; Berger, F.; Schmitt, B. Transcatheter Pulmonary Valve Replacement from Autologous Pericardium with a Self-Expandable Nitinol Stent in an Adult Sheep Model. *J. Vis. Exp.* **2022**. https://doi.org/10.3791/63661.
16. Kang, S.L.; Benson, L. Recent advances in cardiac catheterization for congenital heart disease. *F1000Res* **2018**, *7*, 370. https://doi.org/10.12688/f1000research.13021.1.
17. Kovács, A. 3D Echocardiography: Toward a Better Understanding of Cardiac Anatomy and Function. *J. Vis. Exp.* **2021**. https://doi.org/10.3791/63565.
18. Krishnaswamy, A.; Tuzcu, E.M.; Kapadia, S.R. Integration of MDCT and fluoroscopy using C-arm computed tomography to guide structural cardiac interventions in the cardiac catheterization laboratory. *Catheter. Cardiovasc. Interv.* **2015**, *85*, 139–147. https://doi.org/10.1002/ccd.25392.
19. Kidoh, M.; Utsunomiya, D.; Funama, Y.; Ashikaga, H.; Nakaura, T.; Oda, S.; Yuki, H.; Hirata, K.; Iyama, Y.; Nagayama, Y.; et al. Vectors through a cross-sectional image (VCI): A visualization method for four-dimensional motion analysis for cardiac computed tomography. *J. Cardiovasc. Comput. Tomogr.* **2017**, *11*, 468–473. https://doi.org/10.1016/j.jcct.2017.09.010.
20. Kucukseymen, S.; Arafati, A.; Al-Otaibi, T.; El-Rewaidy, H.; Fahmy, A.S.; Ngo, L.H.; Nezafat, R. Noncontrast Cardiac Magnetic Resonance Imaging Predictors of Heart Failure Hospitalization in Heart Failure With Preserved Ejection Fraction. *J. Magn. Reson. Imaging* **2022**, *55*, 1812–1825. https://doi.org/10.1002/jmri.27932.
21. Ostvik, A.; Salte, I.M.; Smistad, E.; Nguyen, T.M.; Melichova, D.; Brunvand, H.; Haugaa, K.; Edvardsen, T.; Grenne, B.; Lovstakken, L. Myocardial Function Imaging in Echocardiography Using Deep Learning. *IEEE Trans. Med. Imaging* **2021**, *40*, 1340–1351. https://doi.org/10.1109/tmi.2021.3054566.
22. Condado, J.F.; Corrigan, F.E., 3rd; Lerakis, S.; Parastatidis, I.; Stillman, A.E.; Binongo, J.N.; Stewart, J.; Mavromatis, K.; Devireddy, C.; Leshnower, B.; et al. Anatomical risk models for paravalvular leak and landing zone complications for balloon-expandable transcatheter aortic valve replacement. *Catheter. Cardiovasc. Interv.* **2017**, *90*, 690–700. https://doi.org/10.1002/ccd.26987.
23. De Ponti, E.; Morzenti, S.; Crivellaro, C.; Elisei, F.; Crespi, A.; Guerra, L. Motion Management in PET/CT: Technological Solutions. *Curr. Radiopharm.* **2018**, *11*, 79–85. https://doi.org/10.2174/1874471011666180419150440.
24. Liu, H.; Wingert, A.; Wang, J.; Zhang, J.; Wang, X.; Sun, J.; Chen, F.; Khalid, S.G.; Jiang, J.; Zheng, D. Extraction of Coronary Atherosclerotic Plaques From Computed Tomography Imaging: A Review of Recent Methods. *Front. Cardiovasc. Med.* **2021**, *8*, 597568. https://doi.org/10.3389/fcvm.2021.597568.

Curriculum Vitae

My curriculum vitae does not appear in the electronic version of my paper for reasons of data protection.

My curriculum vitae does not appear in the electronic version of my paper for reasons of data protection.

Publications：

Publication 1: Transcatheter Pulmonary Valve Replacement from Autologous Pericardium with a Self-Expandable Nitinol Stent in an Adult Sheep Model.
Hao Y, Sun X, Kiekenap JFS, Emeis J, Steitz M, Breitenstein-Attach A, Berger F, Schmitt B. Transcatheter Pulmonary Valve Replacement from Autologous Pericardium with a Self-Expandable Nitinol Stent in an Adult Sheep Model. J Vis Exp. 2022 Jun 8;(184).
https://doi.org/10.3791/63661 IF: 1.355 (2020)

Publication 2: Four-Dimensional Computed Tomography-Guided Valve Sizing for Transcatheter Pulmonary Valve Replacement.
Sun X*****, **Hao Y***, Sebastian Kiekenap JF, Emeis J, Steitz M, Breitenstein-Attach A, Berger F, Schmitt B. Four-Dimensional Computed Tomography-Guided Valve Sizing for Transcatheter Pulmonary Valve Replacement. J Vis Exp. 2022 Jan 20;(179).
https://doi.org/10.3791/63367 IF: 1.355 (2020)
*Share first authorship.

Publication 3: Straightened Segmentation in 4D Cardiac CT: A Practical Method for Multiparametric Characterization of the Landing Zone for Transcatheter Pulmonary Valve Replacement.
Sun X*****, **Hao Y***, Steitz M, Breitenstein-Attach A, Sebastian Kiekenap JF, Emeis J, Khan MB, Berger F, Schmitt B. Straightened Segmentation in 4D Cardiac CT: A Practical Method for Multiparametric Characterization of the Landing Zone for Transcatheter Pulmonary Valve Replacement. Appl. Sci. 2022, 12, 12912.
https://doi.org/10.3390/app122412912 IF: 2.838 (2021)
*Share first authorship.

Acknowledgement

I would like to express my gratitude to all those who offered great help with my doctoral dissertation.

My deepest gratitude goes first and foremost to my supervisor **PD Dr. Boris Schmitt** for giving me this precious opportunity to study at Charité-Universitätsmedizin Berlin and Deutsches Herzzentrum Berlin. It is an incredible honor to be his doctoral student. He provided me with constant encouragement and guidance in every stage of my doctoral studying. Furthermore, I am also greatly indebted to **Prof. Felix Berger**, who helped me a lot during my doctoral studying time.

Second, my sincere thanks also go to each team member of our group. **Marvin Steitz, Alexander Breitenstein-Attach, Jasper Emeis, Mahamuda Badhon Khan**, their company helped me get through my time in Berlin and made my life colorful. And I would like to express my gratitude to the colleagues who gave instruction and assistance for our animal experiments.

Importantly, my gratitude also extends to **the China Scholarship Council (CSC)** for the generous financial support that enable me to complete my research in Berlin.

Lastly, but by no means least, I would like to express my deep gratefulness to my family, especially my husband, **Xiaolin Sun**, who gave me support from research work to daily life.